Journal of Intelligent Manufacturing
https://doi.org/10.1007/s10845-022-02012-0

A review of machine learning techniques for process and performance optimization in laser beam powder bed fusion additive manufacturing

Jia Liu[1] · Jiafeng Ye[1] · Daniel Silva Izquierdo[1] · Aleksandr Vinel[1] · Nima Shamsaei[2] · Shuai Shao[2]

Received: 27 April 2021 / Accepted: 18 August 2022

Abstract
Laser beam powder bed fusion (LB-PBF) is a widely-used metal additive manufacturing process due to its high potential for fabrication flexibility and quality. Its process and performance optimization are key to improving product quality and promote further adoption of LB-PBF. In this article, the state-of-the-art machine learning (ML) applications for process and performance optimization in LB-PBF are reviewed. In these applications, ML is used to model the process-structure–property relationships in a data-driven way and optimize process parameters for high-quality fabrication. We review these applications in terms of their modeled relationships by ML (e.g., process—structure, process—property, or structure—property) and categorize the ML algorithms into interpretable ML, conventional ML, and deep ML according to interpretability and accuracy. This way may be particularly useful for practitioners as a comprehensive reference for selecting the ML algorithms according to the particular needs. It is observed that of the three types of ML above, conventional ML has been applied in process and performance optimization the most due to its balanced performance in terms of model accuracy and interpretability. To explore the power of ML in discovering new knowledge and insights, interpretation with additional steps is often needed for complex models arising from conventional ML and deep ML, such as model-agnostic methods or sensitivity analysis. In the future, enhancing the interpretability of ML, standardizing a systemic procedure for ML, and developing a collaborative platform to share data and findings will be critical to promote the integration of ML in LB-PBF applications on a large scale.

Keywords Machine learning · Laser beam powder bed fusion · Process and performance optimization · Process-structure–property relationships · Prediction accuracy · Interpretability

Introduction

Additive manufacturing as a viable production alternative

Additive manufacturing (AM), which fabricates complex geometrical 3D objects using layer-wise material deposition directly from digital solid models, is transforming from rapid prototyping to a revolutionary digital manufacturing technology for functional and structural applications (Everton et al., 2016a; Ford & Despeisse, 2016; Guo & Leu, 2013; Rao et al., 2015a). Compared with traditional manufacturing, AM is superior in design flexibility, product customization, low-volume timely production, and cost and lead-time reduction, constituting a viable production alternative for future manufacturing (DeVor et al., 2012; Ford & Despeisse, 2016; Ghobadian et al., 2020; Guo & Leu, 2013).

In the recent decade (2010 ~ 2020), AM technology has been adopted in a variety of industries, such as aerospace, defense, and biomedical. The steep growth projected for the global AM market implies an optimistic prospect of AM to revitalize manufacturing. In 2020, the global AM market value was estimated to be $12 Billion and is expected to grow to $78 Billion by 2028 (Global Additive Manufacturing Market & Technology Forecast 2020).

To secure AM technology as a viable production alternative, a great amount of research effort has been devoted to understanding the process-structure–property (PSP) relationships (Fatemi et al., 2019; Liu et al., 2019; Masoomi

✉ Jia Liu
lzj0040@auburn.edu

[1] Department of Industrial and Systems Engineering, Auburn University, Auburn, AL 36830, USA

[2] Department of Mechanical Engineering, Auburn University, Auburn, AL 36830, USA

Published online: 15 September 2022

et al., 2018; Shrestha et al., 2019; Soltani-Tehrani et al., 2020; Yadollahi et al., 2017) in AM processes and continuously improving product quality (Smith et al., 2016). Applying computational methods, such as simulation and ML, has also been gaining increased attention, especially in the ongoing global process of developing infrastructure with artificial intelligence for future intelligent manufacturing ("Strategy for American Leadership in Advanced Manufacturing", 2018).

Machine learning to improve advanced manufacturing

In the same decade, artificial intelligence (AI) is also experiencing an explosive advancement in both research and applications due to the exponential development in computing infrastructure and ever-increasing data availability. Technological breakthroughs in AI enable intelligent systems to take on increasingly sophisticated tasks and augment human capabilities in new and profound ways. They are improving and reconstructing every aspect of human life, such as finance, communication, and e-commerce (Jordan, 2019; Russell & Norvig, 2003; Tegmark, 2017).

Machine learning (ML), a subset of AI, is widely used for data analysis and decision-making in this data-rich era. It can quickly recognize data patterns from historical data (which could have been neglected by humans), extract insights, and establish data-driven predictive models with high accuracy to facilitate decision-making (Bishop, 2006; Goodfellow et al., 2016; Molnar, 2020; Zhang & Ma, 2012). Depending on their functionality, three commonly used ML paradigms include supervised learning, unsupervised learning, and reinforcement learning (Bishop, 2006). Supervised learning aims to learn the relationships between predictors and response (or the target variable) in the data mainly via regression (with continuous response) and classification (with discrete response); unsupervised learning groups data into different clusters only based on predictors themselves; reinforcement learning explores the optimal solutions in an environment with feedback to maximize the cumulative reward.

AI and ML are gaining increasing attention from the manufacturing community, both in academia and industry. Manufacturing has become the next industry where AI and ML aim to upgrade and reconstruct ("Recommendations for Strengthening American Leadership in Industries of the Future", 2000; Lee et al., 2018; Li et al., 2017). It is foreseeable that new and innovative partnerships with industry and academia will entail an effective transition and translation of ML research outcomes into manufacturing applications at scale.

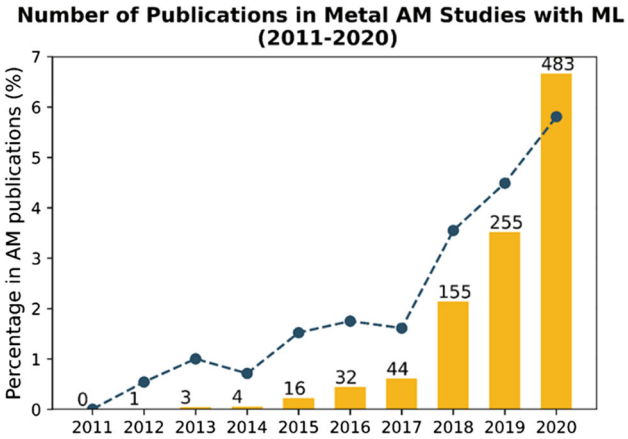

Fig. 1 Total number of research articles and review articles in metal-based AM with ML during 2011–2020 in ScienceDirect (search keywords: ML, metal, AM, 3D printing). It can be seen that in 2020, there are 483 published metal-based AM studies with ML, about 6% of all publications in metal-based AM

Machine learning in additive manufacturing

ML has gained increasing attention in AM research as a way to build surrogates with various sensor data and measurements for the PSP relationships. It has been demonstrated to be a convenient way to perform complex pattern recognition and data-driven analysis without an explicit need to construct and solve the underlying physical models (Bishop, 2006; Breiman et al., 1984; Drucker et al., 1996; Freedman, 2009; Ho, 1995; Tibshirani, 1996). For instance, two ML paradigms—supervised learning and unsupervised learning—are widely used in different AM applications, such as product design, parameter optimization, process monitoring, and quality control (Goh et al., 2021; Meng et al., 2020; Qi et al., 2019; Razvi et al., 2019; Wang et al., 2020).

Since 2011, the progress of integrating ML into AM research has been accelerating. In ScienceDirect, the number of publications (i.e., research articles and review articles) of metal-based AM studies with ML applications has increased from 0 to 483 within the 10 years, as in Fig. 1. The percentage of metal-based AM studies with ML increases rapidly in the recent 3 years and has reached ~ 6% of all the metal-based AM publications in 2020. (Search keywords: ML, metal, AM, 3D printing).

The integration of ML into AM studies also follows the corresponding evolution of ML algorithms. Only linear models (Freedman, 2009; Tibshirani, 1996) are used to quantify the linear relationships among important process variables in AM with experimental data at the early stage. Later, conventional "shallow" ML methods (Breiman et al., 1984; Cortes & Vapnik, 1995; Ho, 1995) are adopted to model the nonlinear relationships among process variables and make predictions

on target variables. Simulation is further applied to augment the experimental training data and improve the training efficiency of ML models. Recently, deep learning models (Bengio et al., 2013; Goodfellow et al., 2016) are adopted to automate feature extraction and achieve even higher prediction accuracy.

With the growth of ML applications in AM studies, several review papers have been published in the last 2 years to organize the state-of-the-art studies from *different perspectives*. To the authors' knowledge, the earliest review work was presented by Razvi et al. (2019) in ASME 2019 International Design Engineering Technical Conferences & Computers and Information in Engineering Conference (IDETC/CIE2019). This paper introduced the newest ML applications in AM along its product lifecycle (including design, process plan, build, post-process, and test and validation). Later, Qi et al. (2019) focused on the current progress of applying neural network (NN) algorithms to AM studies in design for AM (DfAM), in situ monitoring, and quality evaluation.

In 2020, Wang et al. (2020) highlighted the state-of-the-art ML applications in AM design, processing, and production. In the design for AM (DfAM), ML can be leveraged to output new high-performance metamaterials and optimized topological designs. In AM processing, contemporary ML algorithms can help optimize process parameters, examine powder spreading, and conduct in-process defect monitoring. In production, ML can assist practitioners in pre-manufacturing planning, and product quality assessment and control. Goh et al. (2021) highlighted promising AM applications (design, material, process) with ML in biomedical, tissue, and civil engineering, and discussed the potential integration with cloud services and cybersecurity. In contrast, Meng et al. (2020) in 2020 organized the studies according to different ML tasks (i.e., regression, classification, and clustering) and evaluated the performance of various ML algorithms.

While these review papers present various aspects of ML applications in AM studies, some limitations can be noted: firstly, the lack of strong focus and deep exploration about ML applications in a specific AM process, which could be more instructive for readers interested in that process; secondly, the absence of systematic analysis and evaluation of ML applications from the perspective of ML elements (e.g., data availability, feature extraction, model selection, and interpretation); finally, the failure to organize ML algorithms in a suitable way for AM practitioners to understand and select, in that the algorithms are usually organized using ML-specific language (e.g., supervised vs. unsupervised learning, regression vs. classification vs. clustering), rather than through the lens of AM application.

Consequently, we aim to conduct a critical literature review, focusing on the state-of-the-art ML applications for process and performance optimization, specifically in the dominant LB-PBF process in metal AM technology. The process and performance optimization is based on process-structure–property (PSP) relationships of LB-PBF, and their machine learning applications include a variety of process parameters (e.g., laser power, scan speed, layer thickness, hatch spacing), process signatures (e.g., melt pool geometry, thermal profiles), structural features (e.g., microstructure, defects, surface characteristics) and property measurements (e.g., tensile strength, density, fatigue life) as the input and target variables. We will discuss the pros and cons of various ML models for these LB-PBF applications in terms of accuracy, complexity and interpretability, examine the data sources used to train the models, and organize studies in the popular PSP framework in AM. In this way, this work not only presents ML applications accessible to LB-PBF researchers for convenient ML algorithm selection but also uncovers physics insights of LB-PBF to ML researchers, promoting the further adoption and innovation of ML application in LB-PBF studies.

Note that some other important ML applications in AM, such as on process monitoring with sensor data or materials development, will not be included in this review. The following recent reviews of these fields can be suggested (Everton et al., 2016b; Failed, 2017; Liu et al., 2021; Rao et al., 2015b; Tapia & Elwany, 2014; Vulimiri et al., 2020).

Background

Laser beam powder bed fusion process

Among various metal AM technologies, powder bed fusion (PBF) dominates the current global metal AM market. In 2019, the installed PBF units accounted for about 86.5% of all metal AM investments and up 85% of the total revenue ("Additive Manufacturing Market by Technology" AMPOWER Report, 2020), as shown in Fig. 2.

Laser beam powder bed fusion (LB-PBF) works on the principle of consolidating feedstock material in layers towards the fabrication of complex objects through localized melting and resolidification using high-power energy sources, namely a laser beam (Fig. 3). It involves depositing a thin layer of powder onto a build plate, melting the powder with predefined patterns using the laser beam, and constructing a 3D part track after track and layer upon layer. During laser scanning, the chamber is protected from oxidation by introducing an inert gas such as argon or nitrogen, and the build plate is heated at around 80 °C before depositing/melting the powder. After finishing the process, the remaining powder is vacuumed and sieved for later reuse.

Compared with other metal AM processes, LB-PBF can fabricate complex geometries with better part accuracy and

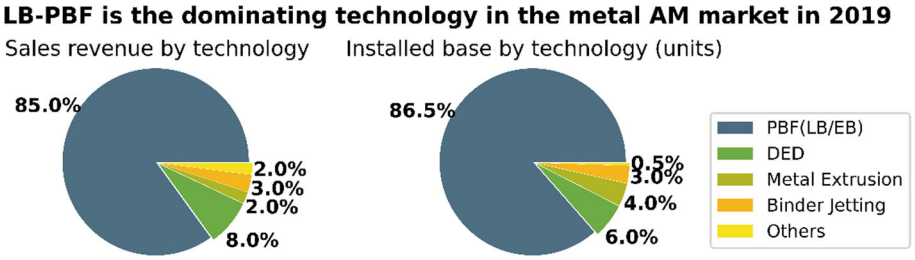

Fig. 2 In 2019, the installed PBF units were about 86.5% among all metal AM technology, and its sale revenue also took up 85% of the total revenue ("Additive Manufacturing Market by Technology" AMPOWER Report, 2020). https://additive-manufacturing-report.com/additive-manufacturing-market/

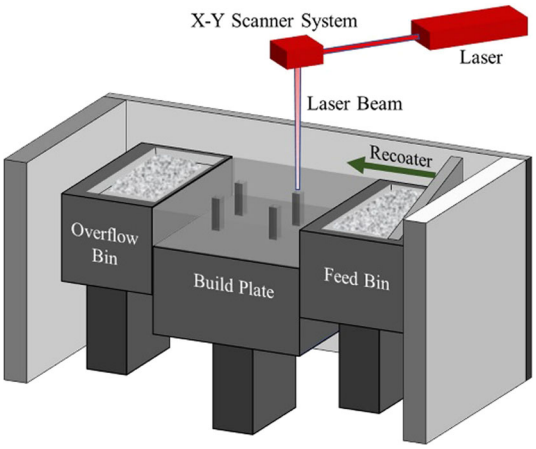

Fig. 3 The sketch of an LB-PBF process (Soltani-Tehrani et al., 2020)

surface finish (Shrestha et al., 2019). The powder bed acts as a supporting mechanism that improves the feasibility of fabricating cantilever-type structures. The powder bed can also reduce thermal gradients, cooling rates, and residual stress by insulating the build and removing convective heat transfer. Additionally, preheating the powder bed before the selective melting stage can yield favorable reductions in residual stress. Yet, LB-PBF has a low utilization rate of powder, and the manufacturing chamber limits the size of its products.

LB-PBF involves complex physics, and its process parameters (such as laser power, scanning speed, powder layer thickness) coupled with other factors (e.g., design, feedstock) govern microstructural traits and mechanical properties of LB-PBF products (Molaei et al., 2020; Pegues et al., 2020; Yadollahi & Shamsaei, 2017). During selective melting, the laser moves at a relatively high speed and has to deliver a very high power density to melt the metal powder, which partially remelts the previously consolidated layer. This process typically leads to a highly dynamic melt pool, ultra-high solidification/cooling rates, and strong epitaxial and directional grain growth. Common microstructural traits of LB-PBF products consist of varying levels of porosity, fine (possibly martensitic) microstructure, and highly texturized, well-aligned grain structures. These microstructural traits and their associated stress concentrations affect the mechanical performance of LB-PBF parts. For instance, the lack-of-fusion (LoF) defects tend to be aligned perpendicular to the build direction, leading to strong anisotropy in tensile and fatigue strength; under fatigue loading, pores and LoF defects often serve as crack initiation sites and can greatly reduce the fatigue life of LB-PBF parts (Yadollahi et al., 2017).

Process-structure–property relationships in LB-PBF

While LB-PBF has a promising potential in complementing or even substituting traditional manufacturing with its fabrication flexibility, the understanding of the governing physics of LB-PBF and the effect of the process on final product performance must be strengthened to increase the level of confidence in promoting LB-PBF in mission-critical applications (Russell et al., 2019). Constructing a linkage between process (P) parameters, structure (S) and properties (P), also known as process-structure–property (PSP) relationships of LB-PBF, is required for scientists and engineers to optimize the process and improve product quality in LB-PBF.

However, the LB-PBF fabrication involves multiscale multi-physics processes, including powder-laser interaction at the microscale, melt pool dynamics and columnar grain growth at the mesoscale, and thermal–mechanical coupling at the macroscale (Markl & Körner, 2016; Sames et al., 2016). The strongly non-equilibrium processes, stemming from melt pool flow, energy deposition, and phase transformations, are of particular importance. Hence, a deep and comprehensive understanding of the PSP relationships in LB-PBF fabrication is extremely challenging.

Experimental approaches, which involve trial and error, can be implemented to investigate the PSP relationships in LB-PBF. However, experiments are usually time-consuming and costly. Further, the limited experimental data is often insufficient to fully capture the complex PSP relationships.

Consequently, it is impractical to obtain reliable models merely by experimental methods since many process parameters are involved in LB-PBF fabrication and their interactions are unknown.

Computational simulation helps understand physical mechanisms, predict fabrication quality, and guide design and optimization in LB-PBF (King et al., 2015; Smith et al., 2016). The physics-based computational simulation can reveal the underlying mechanism of specific features during fabrication, such as melt pool geometry, keyhole, and microstructure. There are macro-scale simulation methods (e.g., continuum-based thermal models) and mesoscale level techniques (e.g., computational fluid dynamics (CFD) models) (Masoomi et al., 2018). The macro-scale simulation enables part-scale modeling and maps complex PSP relationships with simplified assumptions and inexpensive computation. For instance, finite element modeling (FEM) methods can simplify the powder bed as a continuum material and incorporate heat transfer but not fluid flow. However, they often suffer from discrepancies with experimental results due to the simplified assumptions and the lack of information about physical properties. In comparison, high-fidelity mesoscale level techniques, e.g., CFD models, resolve the thermofluid flow behaviors of individual powder particles. As a result, their computation time can be prohibitively high to simulate and predict the mechanical properties on the part scale.

The multi-physics multiscale LB-PBF process makes it nearly impossible to model the PSP linkage quickly and accurately with experiments or simulation alone. Hence, there is a strong need for efficient and effective analytical surrogates to approximate the PSP relationships in LB-PBF.

Introduction of ML in LB-PBF

With the increase of the amount of available sensing and testing data, ML becomes an effective candidate to explore and understand complex PSP relationships in LB-PBF in a data-driven way. It uses historical data to train surrogate models, which identify correlation among process variables, approximate PSP relationships, and make predictions. Such data-driven ML modeling can overcome the limitations of experimental designs and computational simulation in model complexity and computational expense. We will focus on ML applications in process and performance optimization for LB-PBF.

Organizing ML algorithms for LB-PBF

To demystify ML algorithms for LB-PBF researchers in this paper, we organize them into three categories: (1) interpretable ML, (2) conventional (shallow) ML, and (3) deep ML, and evaluate them in four practical dimensions: accuracy, complexity, interpretability, and data requirement, as shown in Fig. 4. In contrast to the traditional ML paradigms (e.g., regression, classification, or clustering), this new way is more straightforward and understandable for practitioners to select suitable ML algorithms for their applications.

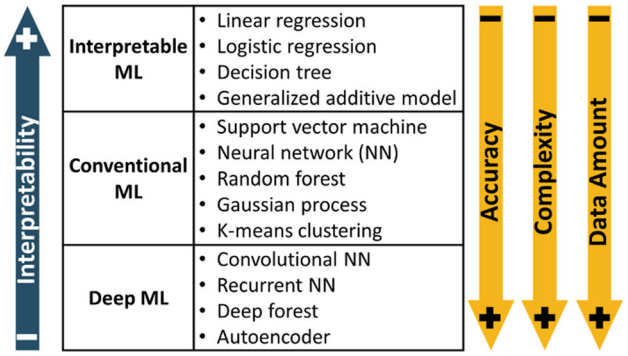

Fig. 4 Three categories of ML algorithms in LB-PBF applications. Generally speaking, the increase of model complexity requires a large amount of data to achieve high prediction accuracy but compromises model interpretability

(1) Interpretable ML (Rudin, 2019), rooted in regression modeling and rule-based ML, regularizes model forms by useful model assumptions (e.g., linearity), structural domain knowledge (e.g., monotonicity, causality, additivity), or physic-based domain knowledge. The interpretable ML methods (e.g., linear regression, logistic regression, decision tree) can establish simple linear models between the predictors and the response with high interpretability. They are beneficial to discover knowledge and justify model predictions (Adadi & Berrada, 2018). However, the model accuracy can be inferior when the relationships between predictors and response are overly nonlinear.
(2) Conventional (shallow) ML (e.g., random forest, support vector machine, artificial neural networks, Gaussian process) emphasizes predictive performance rather than interpretability. They can model nonlinear relationships between predictors and response by "black-box" models. However, it is of importance for conventional ML to transform the raw data into suitable internal representation by careful feature engineering.
(3) Deep ML, such as deep neural networks, can learn complex functions or relationships between input data and output variables and achieve high prediction accuracy. They are composed of multiple processing layers with simple but nonlinear modules to transform the representation at one level (starting with the raw input) into a representation at a higher, more abstract level. Higher layers of representation amplify aspects of the input that

are important for discrimination and suppress irrelevant variations. With the composition of such nonlinear transformations, complex functions can be learned from data using a general-purpose learning procedure, but the interpretation of output variables from input data is challenging.

With the increase of complexity in ML models, a large amount of training data is required to achieve high prediction accuracy, but the interpretability decreases ("Broad Agency Announcement and Explainable Artificial Intelligence (XAI)," Defense Advanced Research Projects Agency 2016). Moreover, for interpretable ML and conventional ML, the input features are selected or engineered manually. In contrast, deep ML can automatically extract features from the raw data. As convenient as it is, deep ML further complicates the model and requires additional steps to increase the interpretability. In addition, ensemble modeling by integrating multiple base ML models is used in some LB-PBF applications to reduce the generalization error of prediction. It seeks the wisdom of crowds in making the prediction. As long as the base ML models are diverse and independent, the prediction error decreases when the ensemble approach is used.

Data sources for ML in LB-PBF

For process and performance optimization with ML algorithms, the available data characterize various aspects of LB-PBF, mainly including (1) process parameters (e.g., energy input, scanning strategies); (2) material specifications; (3) process signatures (e.g., melt pool geometry, thermal history); (4) structure of LB-PBF parts (e.g., defects, surface roughness, microstructure); (5) properties and performance on LB-PBF parts (e.g., density, tensile strength, fatigue life) (Popova et al., 2017; Smith et al., 2016). They are used to build surrogate models by ML in a data-driven manner to approximate the PSP relationships in LB-PBF.

These data are generated from experiments or simulations (Everton et al., 2016a; Smith et al., 2016). The experimental measurements include both destructive methods (such as scanning electron microscopy, optical tomography) and non-destructive ways (such as X-ray radiography and CT, ultrasonic techniques). Specifically, image-based data regarding process signatures (e.g., melt pool) and structure (e.g., microstructure, defects, surface roughness) of LB-PBF parts entail detailed information about the fabrication process and the products. The diversity of measurements promotes applications of cutting-edge ML algorithms such as deep learning in LB-PBF. Due to the expensive data acquisition from experiments, simulation is sometimes also used to generate the training data for ML models. Furthermore, the simulated data can be integrated with experimental data to improve model accuracy.

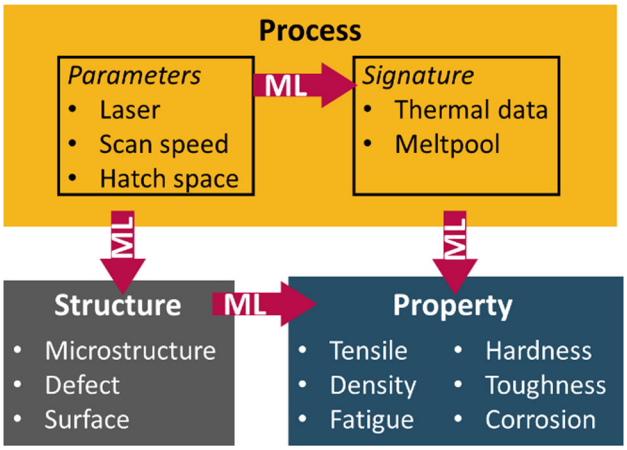

Fig. 5 The reviewed ML applications in LB-PBF for process and performance optimization are organized in the PSP framework according to their targeted relationships, indicated by the red arrows (Color figure online)

ML for process and performance optimization in LB-PBF

In this section, we will review current ML applications for the LB-PBF process and performance optimization. They use ML methods to extract hidden patterns in historical data, approximate and understand the PSP relationships, and make predictions in a data-driven way.

The reviewed studies are organized according to their targeted relationships in the PSP framework, namely, (1) process parameters—process signature, (2) process—structure, (3) process—property, and (4) structure—property, as shown in Fig. 5. For each targeted relationship, we will further group and review papers in terms of a specific response. For instance, when reviewing studies modeling the process-structure relationship, the studies investigating how process parameters affect defects are evaluated together. Such organization can reveal underlying physical mechanisms in these relationships, augmenting the evaluation of different ML methods with domain knowledge.

ML algorithms will be evaluated in terms of their categories (i.e., interpretable ML, conventional ML, and deep ML) defined in section "Introduction of ML in LB-PBF", along the four dimensions of complexity, accuracy, interpretability, and data requirement. The interpretability of models is particularly important to understand the process and performance optimization. Data sources (i.e., experimental, simulation, or hybrid) and feature selection/extraction (manual or automatic) for each study will also be introduced.

Table 1 ML applications to model and utilize process parameters—signature relationship in LB-PBF

Materials	Input	Output	Models	Categories	Data	References
Alloy 718	Laser power, scanning speed	Melt pool geometry	Linear regression, polynomial regression	Interpretable ML	Experiment	Scime & Beuth, (2019); Sadowski et al., (2016)
Alloy 625, alloy 718	Powder properties, size distribution, layer thickness, laser parameters	Melt pool geometry	Bayesian ridge regression, kernel ridge regression, linear regression, nearest neighbors, random forest, support vector machine	Interpretable ML, Conventional ML	Experiment	Molnar, (2020)
316L SS	Laser power, beam size, scanning speed, absorptivity	Melt pool geometry	Regression tree, Gaussian process	Interpretable ML, Conventional ML	Simulation	Kamath, (2016)
316L SS	Laser power, beam size, scanning speed, absorptivity	Melt pool geometry	Regression tree, locally weighted kernel regression, ensemble tree, multivariate adaptive regression splines, support vector regression, Gaussian process	Interpretable ML, Conventional ML	Simulation	Kamath & Fan, (2018)
	Laser power, scanning speed, laser spot diameter, absorptivity, layer thickness	Melt pool geometry	Gaussian process	Conventional ML	Simulation	Olleak & Xi, (2020)
316L SS	Laser power, scanning speed, beam size	Melt pool geometry	Gaussian process	Conventional ML	Hybrid	Tapia et al., (2018)
17–4 PH, 316L SS	Laser power, scanning speed	Single-track depth	Gaussian process	Conventional ML	Simulation	Meng & Zhang, (2020)
	Laser power, temperature	Melt pool size	Gaussian process	Conventional ML	Hybrid	Ren & Wang, (2021)
	Laser power, scan speed, absorption, thermal diffusivity	Melt pool size	Gaussian process	Conventional ML	Simulation	Yang et al., (2018a)
316L SS	Laser power	Melt pool geometry	Deep neural networks	Deep ML	Experiment	Kwon et al., (2020)
	Laser power, scanning speed	Melt pool geometry	Gaussian process	Conventional ML	Simulation	Mondal et al., (2020)
Ti-6Al-4V	Laser power, laser speed, hatch spacing	Thermal histories	Support vector regression	Conventional ML	Simulation	Srinivasan et al., (2020)
Ti-6Al-4V	Laser power, laser speed,	Track morphologies, bead characteristics	Random forest, ANN	Conventional ML	Experiment	Le-Hong et al., (2021)

Table 1 (continued)

Materials	Input	Output	Models	Categories	Data	References
	Laser power, spot diameter, scan speed, beam focus position, laser point distance, layer thickness, hatch spacing, powder bed temperature	Track quality	Convolutional autoencoder, K-means clustering	Deep ML, Conventional ML	Experiment	Tibshirani, (1996)

ML in process parameters—process signature relationship

LB-PBF process signatures, such as melt pool characteristics and thermal history, are directly affected by process parameters and indicative of the structure and properties of LB-PBF products. Therefore, many studies use ML methods to discover the relationship between process parameters and process signatures and use the relationship to optimize the process, as listed in Table 1.

Optimize process parameters according to desired melt pool morphology

A melt pool is formed from the melting of powder particles by the laser. The cross-sectional morphology of the melt pool records the interaction between laser and metal powder during fabrication. The impact of process parameters (mainly laser power and speed) on the melt pool morphology is investigated using ML methods.

Interpretable ML methods are used to linearly relate the process parameters to the melt pool geometry (e.g., width, depth, area within the substrate, height) post-fabrication. For instance, Scime & Beuth (2019) mapped the melt pool cross-sectional geometry to the combinations of laser power and scanning speed on LB-PBF Inconel 718 alloy using linear regression. The cross-sectional width, depth, and area were measured using microscopy on 720 melt tracks under 36 different process parameter combinations. Also, with Inconel 718 alloy, Sadowski et al. (2016) printed 24 square LB-PBF specimens under different combinations of laser power and scanning speed from a full factorial experimental design, and used a polynomial regression model to understand the effect of process parameters on scan line quality and melt pool geometry. The linear energy density, the ratio of laser power to scanning speed, was introduced to model the second-order polynomial trend line for melt pool width with high fidelity ($R^2 \geq 0.92$).

Apart from laser power and scanning speed, other process parameters and material properties are also included in the interpretable ML models as input features. For instance, Lee et al. (2019) used 23 input features of LB-PBF, including chemistry of powders (alloy 625 and alloy 718), materials thermal property (solidus, liquidus, density, conductivity, thermal diffusivity, specific heat), powder size distribution, layer thickness and laser parameters (power, scan speed, energy density, beam diameter) to model 5 responses of melt pool geometry (i.e., width, depth, area within the substrate, height, area based on the height). More data were required in training with the increase of input features, and the melt pool geometry for 472 single tracks was measured. Bayesian ridge regression, kernel ridge regression, and linear regression can model linear relationships with high interpretability.

Moreover, to reduce the cost for experiments, simulated data are also used for investigating the relationships between process parameters and melt pool geometry. For instance, Kamath (2016) used simulated data of melt pool depth for LB-PBF 316L stainless steel based on process parameters (laser power, speed, beam size, and absorptivity) to develop a predictive model with a regression tree. Later, Kamath & Fan (2018) generated training data of melt pool geometry from two simulations (i.e., Eagar–Tsai and Verhaeghe) with different parameter combinations of scanning speed, laser power, beam size and absorptivity. Three regression tree models were trained with 462, 100, and 41 simulated data points, respectively. The prediction error of melt-pool characteristics for LB-PBF from the regression tree can be as low as 1.92%.

Conventional ML methods are trained with historical data to make predictions on melt pool geometry according to process parameters. For instance, Lee et al. (2019) used a variety of conventional ML approaches, such as nearest neighbor clustering, random forest, support vector machine (SVM), to facilitate reliable prediction of melt-pool geometries for alloy 625 and alloy 718 from 23 input features of power and process parameters. Trained on 472 single tracks, the results showed that SVM and nearest neighbors outperform other ML models in terms of prediction accuracy. However, the physics-based interpretation was challenging with these conventional ML models.

Kamath & Fan (2018) built reliable surrogate models to predict the melt-pool characteristics for LB-PBF from process parameters by different ML algorithms, including locally weighted kernel regression (LWKR), ensemble tree, multivariate adaptive regression splines (MARS), support vector regression (SVR), and Gaussian process (GP). The input of surrogate models was process parameters, including scanning speed, laser power, beam size, and absorptivity, and the output is length, width, depth of melt pools. Three training datasets were generated from simulations (Eagar–Tsai and Verhaeghe). In comparison, the GP-based surrogate model provided the best prediction accuracy (> 99%) and was the easiest to use in practice, even with a small dataset.

Particularly, GP modeling is a popular and convenient method for modeling melt pool characteristics based on process parameters with experimental and simulated data. The covariance matrix of GP implies that similar values of process parameters can lead to similar melt pool characteristics. For instance, by using simulated data, Kamath (2016) developed a Gaussian process to predict the melt pool depth for LB-PBF 316L stainless steel based on process parameters (laser power, speed, beam size, and absorptivity) with low prediction error (~ 3%). Olleak & Xi (2020) developed a GP regression metamodel for high-fidelity melt pool size prediction from process parameters of LB-PBF (laser power, scanning speed, laser spot diameter, absorptivity, layer thickness) with 94 FEM-simulated data. With the implication of the GP covariance matrix, the metamodel can be calibrated to high accuracy with experimental data of small size.

Tapia et al. (2018) proposed a GP-based surrogate model of the LB-PBF process that predicts melt pool depth in singletrack experiments given laser power, scan speed, and laser beam size. The authors developed a GP surrogate model from 96 experimental data of 316L stainless steel and 26 simulation data, with prediction errors less than 10%, respectively, as in Fig. 6. Later, Meng & Zhang (2020) developed a GP regression model to predict the remelted depth of single tracks of LB-PBF 17–4 PH as a function of laser power and scanning speed. The GP model was trained by 24 simulated data from a computational fluid dynamics (CFD) model. The mean absolute prediction error from the GP model was only 0.6 um for a powder bed with a layer thickness of 30 um. Ren & Wang (2021) modeled melt-pool dynamics for multitracks built with L-PBF AM processes by GPR with both experimental and simulated data of laser power and melt pool tempeature. The achieved R^2 on the prediction of melt pool size is about 96%. Then a (sub)optimal control of laser power, derived using a projected gradient descent algorithm, was applied to regulate themelt-pool size to a constant reference value with a RMSE of ~ 10%.

Lastly, to dynamically predict the melt pool size of LB-PBF from process parameters, the GP model can be further improved by adjusting the covariance matrices with simulated data. For instance, Yang et al. (2018a) proposed a dynamic variance–covariance matrix (DVCM) method by incorporating dynamic covariance matrices into the GP regression to deal with large and nonideal datasets in manufacturing scenarios. DVCM method was used to build a metamodel for predicting the melt pool size of LB-PBF from process parameters (laser power, scan speed, absorption coefficient, and thermal diffusivity). A total of 1,050 data points were simulated from a full factorial design of experiments. The prediction error was less than 0.03%. Besides, Mondal et al. (2020) developed a GP regression surrogate model to predict time-dependent melt pool geometry during the LB-PBF fabrication process based on laser power and scanning speed. The model was trained using 200 Eagar-Tsai simulated values of melt pool depth and width at each time instant with different combinations of laser power and scanning speed.

Optimize process parameters with other process signatures

Conventional ML is also used to optimize LB-PBF process parameters with the thermal histories of LB-PBF. For instance, Srinivasan et al. (2020) integrated support vector regression and optimization to identify scan parameter sets (i.e., laser power, laser speed, and hatch spacing) that produce similar local processing histories in LB-PBF Ti-6Al-4V specimens. The local thermal histories of reference tiles were simulated from a physics-based analytical thermal model under different combinations of process parameters. These local thermal histories underwent dimensionality reduction by principal component analysis and partitioning by density-based spatial clustering to form a reference parameter-thermal history "map". The scan parameter sets for arbitrary part geometry can be projected onto this "map" and iteratively optimized to ensure similar local thermal histories.

Le-Hong et al. (2021) investigated the effects of two key process parameters of SLM (i.e., laser power and scanning speed) on the single-track morphologies and the bead characteristics, especially the depth-to-width D/W and height-to-width H/W ratios using ML approaches (i.e., random forest and ANN). Both models could predict reasonably well the two aspect ratios, D/W and H/W, with an overall R^2 value reaching about 90%, respectively.

When a large amount of image data is available, deep ML can be a viable candidate to facilitate feature extraction and formulate accurate predictive models. For instance, Silbernagel et al. (2019) explored a convolutional autoencoder-based process parameter optimization for LB-PBF copper specimens with 47,488 optical images of single scan tracks from different parameter combinations (laser power, laser spot diameter, powder bed temperature, laser scan speed,

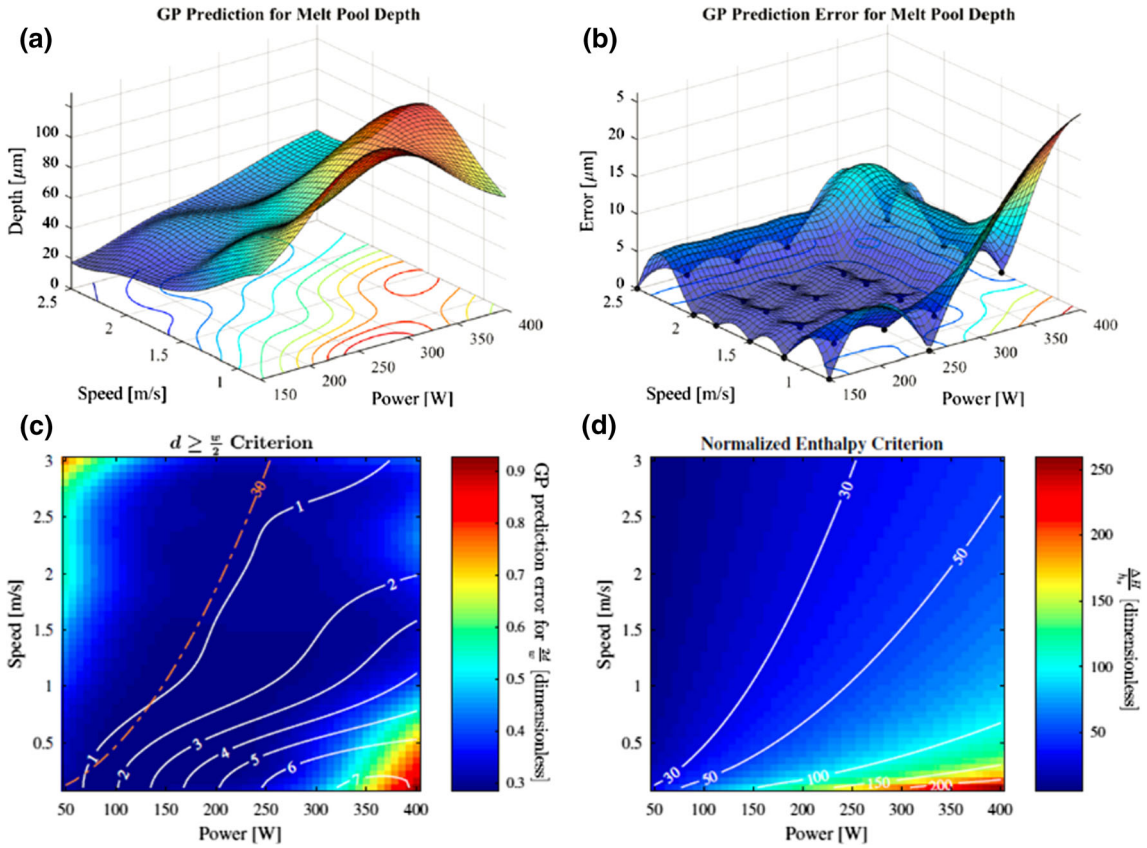

Fig. 6 Visualization of results for the GP model trained with simulation dataset **a** mean value of the predictions and **b** standard deviation of the prediction. L-PBF process windows specifying condition and keyhole mode behavior with $d \geq \frac{w}{2}$ criterion in **c** and normalized enthalpy $\frac{\Delta H}{h_s} \geq 30$ criterion in (**d**). The color scale on the right bar represents the standard deviation of the GP predictions, while the figures on the white contour lines display the mean value of the GP prediction (Tapia et al., 2018) (Color figure online)

laser point distance, layer thickness, laser beam focus position, and hatch spacing). These images were labeled according to the track quality (e.g., continuous, discontinuous, balling), and fed into the proposed convolutional autoencoder. The output features were then clustered by a k-means mini-batch algorithm to find high-quality clusters with feasible process parameters. The results from this deep ML aligned with many observations in the traditional parameter optimization process on deciding the optimal laser point distance, powder layer thickness, and laser scanning speed. Kwon et al. (2020) applied a deep neural network (10 hidden layers neural network with 360 nodes) to classify melt-pool images with respect to six laser power conditions and achieved a classification failure rate under 1.1% for 13,200 test images.

ML in process—structure relationship

Adjusting process parameters can lead to different structural properties of LB-PBF products (such as surface roughness, porosity, and microstructure). In this section, ML applications exploring the relationships between process and structure are reviewed, as in Table 2. We noticed there are three highlights in the ML applications:

(a) Interpretable ML is mostly used to evaluate the impact of process parameters on the LB-PBF part structure;
(b) Conventional ML, especially artificial neural networks (ANN), is adopted to model complex relationships and make accurate predictions;
(c) Clustering is applied for both data preprocessing and modeling.

Process and performance optimization with LB-PBF structural traits

Many studies investigate process parameters' impact on surface roughness and porosity, two preeminent structural traits of LB-PBF products. For instance, Gockel et al. (2019) fabricated fourteen as-built LB-PBF alloy 718 coupons with

Table 2 ML applications to model and utilize process—structure relationship in LB-PBF

Materials	Input	Output	Models	Categories	Data	References
Alloy 718	Laser power, scanning speed	Surface roughness, internal defects	Linear regression	Interpretable ML	Experiment	Gockel et al., (2019)
Alloy 718	coupon position, orientation, fraction recycled powder, laser incidence angles	Porosity	Random forest	Conventional ML	Experiment	Kappes et al., (2018)
Ti-6Al-4V	Laser power, scanning speed, layer thickness, hatch distance	Surface roughness, density	ANN	Conventional ML	Experiment	Park et al., (2022)
CoCr alloy	Beam current and scanning speed (EB-PBF)	Surface roughness, porosity	Support vector machine (SVM)	Conventional ML	Experiment	Aoyagi et al., (2019)
Alloy 718	Length, sphericity, aspect ratio of pores	Porosity	K-means clustering	Conventional ML	Experiment	Snell et al., (2020)
316L SS	Laser power, scanning speed, beam size	Keyhole mode	Gaussian process	Conventional ML	Hybrid	Tapia et al., (2018)
17–4 PH, 316L SS	Laser power, scanning speed	Keyhole mode	Gaussian process	Conventional ML	Simulation	Meng & Zhang, (2020)
	Laser power, scan speed, layer thickness	Open porosity	Ensemble of ANN, Bayesian classifier, SVM	Conventional ML	Simulation	Garg et al., (2015)
	Scan pattern, velocity, melt pool	Microstructures	Multivariate polynomial regression	Interpretable ML	Experiment	Popova et al., (2017)
	Build directions, orientations	Shrinkage rate	Linear model	Interpretable ML	Experiment	Yang et al., (2002)
	Layer thickness, laser power, scanning speed, scanning mode, hatch spacing, interval time, surrounding temperature	Shrinkage ratio	Artificial neural network (ANN)	Conventional ML	Experiment	RongJi et al., (2009)
	Powder bed support, laser spot size, remelting depth of heat source	Shape deviations	Artificial neural network (ANN)	Conventional ML	Simulation	Hong et al., (2020)
316L SS	Laser power, spot diameter, scan speed, beam focus position, laser point distance, layer thickness, hatch spacing, powder bed temperature	Lattice deformation	Convolutional neural networks (CNN)	Deep ML	Experiment	Garland et al., (2020)

Table 2 (continued)

Materials	Input	Output	Models	Categories	Data	References
Ti-6Al-4V	Spreader translation speed, spreader rotation speed	Powder mass, spread throughput, layer roughness, layer porosity	Artificial neural network (ANN)	Conventional ML	Simulation	Desai & Higgs, (2019)
Ti-6Al-4V	Spreader translation speed, spreader rotation speed	Powder layer roughness, layer porosity	Artificial neural network (ANN)	Conventional ML	Simulation	Zhang et al., (2017)
Ti-6Al-4V	Thermal signature of surface	Subsurface porosity	Logistic regression, random forest, gradient boosting, Gaussian process	Interpretable ML, Conventional ML	Experiment	Paulson et al., (2020)
Ti-6Al-4V	Thermal histories	Microstructure	K-means clustering	Conventional ML	Simulation	Donegan et al., (2020)

different combinations of process parameters and found that laser power and scanning speed could linearly impact surface roughness and internal defects within an operating window.

Conventional ML methods are more popular, as they offer high prediction accuracy to model the complex process—structure relationships. For instance, Kappes et al. (2018) investigated the impact of process parameters (coupon position, orientation, fraction recycled powder, and laser incidence angles) on the porosity of LB-PBF Inconel 718. The laser settings, laser scan path, and layer thickness were kept at the manufacturer's recommendation. A random forest network (RFN) was trained by pores of LB-PBF specimens scanned from X-ray CT. The results revealed that the orientation of the part had the greatest effect on the pore population while the position on the plate, transverse to the blade direction, had the greatest impact on the median pore size and distribution.

Park et al. (2022) applied ANN with four key process parameters (laser power, scanning speed, layer thickness, and hatch distance) to predict two target properties of a part fabricated by the SLM technique (density ratio and surface roughness). The model's performance was proven with a value of R^2 of 99% for both density ratio and surface roughness.

Aoyagi et al. (2019) constructed a process map for electron beam powder bed fusion (EB-PBF) CoCr alloy specimens using a support vector machine (SVM), predicting surface roughness and porosity of specimens from two process parameter combinations (beam current and scanning speed). The SVM model was trained by 11 fabricated cylinders, which were classified into two classes (good or bad) according to pore radii and surface morphology. The median error rate for the prediction was as low as 0.09.

Snell et al. (2020) formulated a pore classification method based on k-means clustering for LB-PBF specimens to differentiate gas pores, keyholes, and lack of fusion. 2D pore data of 81 LB-PBF Inconel 718 specimens are obtained from micrographs, and the roundness and length of 21,955 pores are used as input for k-means clustering. 3D pore data of LB-PBF Ti-6Al-4V specimens were obtained from X-ray computed tomography; the length, sphericity, and aspect ratio were used to cluster 2664 pores. The results in Fig. 7 showed that 3D pore data clustering performed well compared with the traditionally defined limits approaches.

Moreover, GP modeling was also used to identify keyhole regimes on the laser power and scanning speed combination for LB-PBF. Tapia et al. (2018) proposed a GP-based surrogate model that mapped the keyhole melting controlled regimes onto a power versus scan speed diagram. The GP surrogate model was trained from 96 experimental data of 316L stainless steel and 26 simulation data given laser power, scan speed, and laser beam size combination. Meng and Zhang (2020) also developed a GP regression model to identify the keyhole mode from laser power and scanning speed for LB-PBF 316L and 17–4 PH stainless steel. The GP model was trained by 24 simulated data from a computational fluid dynamics (CFD) model as a function of laser power and scanning speed.

Ensemble modeling, which combines several individual ML algorithms to improve prediction accuracy, is used in complex process-structure relationships. Garg et al. (2015) presented multi-gene genetic programming (MGGP) combining with ANN, Bayesian classifier, and SVM algorithm to predict the open porosity in LB-PBF products with the combination of three process parameters (layer thickness, laser power, and laser scan speed). The results showed that the two

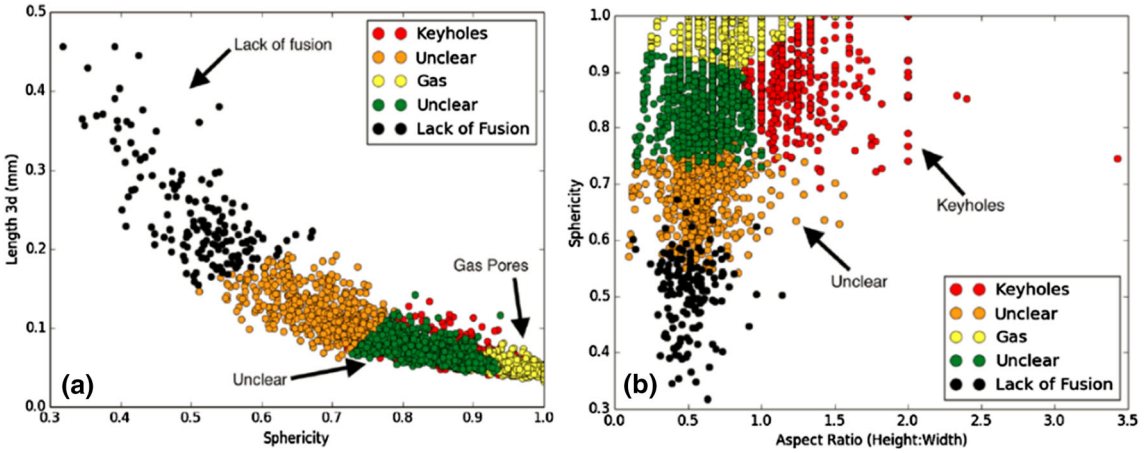

Fig. 7 Pore classification based on k-means clustering for LB-PBF specimens to differentiate gas pores, keyholes, and lack of fusion for the 3D pore data: **a** clustered results based on pore length and sphericity; **b** clustered results based on sphericity and vertical aspect ratio (Snell et al., 2020)

process variables (the laser power and laser scan speed) had the highest impact on the open porosity.

For the microstructure of LB-PBF parts, Popova et al. (2017) introduced a novel data science workflow to investigate the process-structure linkages. A set of 1799 individual synthetic microstructures from the Potts-kinetic Monte Carlo model were simulated by varying process parameters (e.g., scan pattern, velocity, and melt pool). Chord length distributions from microstructures were selected as the features with dimensionality reduction by principal component analysis (PCA). Multivariate polynomial regression was used to establish a surrogate model for the final microstructure from the process parameters with a high goodness of fit ($R^2 > 90\%$) and prediction accuracy (MAE < 0.05).

Inference on LB-PBF structure from process signatures

Process signatures such as thermal history can be used in ML models to infer the structure traits of LB-PBF parts. For example, Paulson et al. (2020) used several ML methods, such as logistic regression, random forest, gradient boosting classification, and GP classification, to learn correlations between the thermal history of prints and subsurface porosity in LB-PBF Ti-6Al-4V for qualification and certification. Fifteen specimens were built with different combinations of laser power, scan speed, scan strategies, and laser spot sizes. The thermal signature of the surface was measured using a fixed infrared (IR) camera, while porosity formation was observed through synchrotron-based high-speed x-ray imaging. ML methods were used to connect features from IR images to the response (large and low porosity, no porosity) and achieved a test accuracy of more than 87.5%.

Donegan et al. (2020) developed a K-means clustering-based zoning procedure to label regions of an LB-PBF Ti-6Al-4 V component such that areas with similar processing were categorized under the same label. Zoning process history can provide insight into the formation of microstructures at different regions and measurement locations. They simulated thermal histories for 11 different geometries from a discrete source model and examined the local thermal history for each point in a 0.1 s temporal and 2 mm spatial window. The high-dimensional thermal histories were processed by symbolic aggregate approximation (SAX) for dimensionality reduction and then clustered by K-means clustering to produce zoned maps of processing thermal history.

Process and performance optimization with LB-PBF geometry

Process parameters (such as laser power, scanning speed, powder thickness, build direction) are used as input for ML methods to compensate for the geometry of LB-PBF parts. For instance, Yang et al. (2002) utilized the analysis of variance (ANOVA) to investigate the impact of building positions of LB-PBF parts on shrinkage rate and formulate scale factors to maintain dimensional accuracy against the changes in the build positions. 27 experiments designed from the Taguchi method with 13 controllable variables (i.e., build directions, orientations) were implemented. The scale factors were a linear combination of selected levels of controllable variables from ANOVA outcomes. On average, the dimensional accuracy with the obtained scale factors could be improved by approximately up to 24% compared to other commercially available methods.

Artificial neural networks (ANNs) provide more flexibility in compensating part geometry from process parameters than the linear ML models. RongJi et al. (2009) applied an ANN to model the shrinkage ratio of LB-PBF components from different process parameters, such as powder layer thickness, laser power, scanning speed, scanning mode, hatch spacing, interval time, and surrounding temperature. The ANN model had 7 input variables (process parameters), one hidden layer with 8 nodes, and the single output of shrinkage ratio. It was trained from 27 data points, had an average relative error of 0.066 on 6 testing data points. Furthermore, a genetic algorithm (GA) was applied to optimize the process parameters to yield minimum shrinkage.

Hong et al. (2020) proposed using an ANN to compensate for truss lattice structures with circular cross-sections printed by LB-PBF. The designed lattice dome structures had five building overhang angles and six platform orientation angles, where overhang angles were influenced by the support of the powder bed, laser spot size, and remelting depth of the laser heat source. Point cloud data from the 3D stereolithography (STL) model and X-ray CT scans (20,000–40,000 data points) were used to train the proposed ANN model, which was based on a multilayer perceptron (MLP) architecture with an input layer of two input variables, one hidden layer of 40 neurons and an output layer. Experimental results showed that ANN improved the cross-sectional area significantly and resulted in a more improved roundness for the trusses than analytical compensation approaches. Moreover, the ANN compensation method can generate free-form lattice cross-sections to compensate local shape deviations more easily, thereby improving the agreement between the as-printed compensated structures and the as-designed ones.

Moreover, deep ML is used to predict part deformation by combining process parameters with designs. For instance, Garland et al. (2020) used convolutional neural networks (CNN) to predict the deformation of lattice structures printed by LB-PBF 316L stainless steel. The CNN algorithm directly related imaging to physical properties. It was trained by ~ 4000 height maps of a total of 96 lattices by varying laser power and scan speed, and it can predict a lattice's deformation with a mean error of 4 ~ 7%. To increase the interpretability of the deep ML model, the authors examined the active convolutions of each layer and the gradient of the kernel weights with respect to the predicted value enables visualization of the key features within an image that influenced the prediction.

Optimization of spreader parameters for LB-PBF powder layer quality

Process parameters of LB-PBF powder spreader (such as spreader speeds) are also used in ANNs to investigate spread layer quality (such as surface roughness and porosity of each powder layer). For instance, Desai & Higgs (2019) proposed a feed-forward, backpropagation neural network surrogate model to study the relationship between spreader speeds and spread layer properties of an industrial-grade Ti-6Al-4V powder, as shown in Fig. 8. The neural network was employed to interpolate between the highly nonlinear results obtained by the discrete element method (DEM) simulations. It had two input variables (spreader translation speed, spreader rotation speed), one hidden layer with 200 nodes, and four output properties, i.e., the mass of powder in the sampling region, spread throughput, roughness of the spread layer, and porosity of the spread layer. It was trained by 50 virtual spreads from DEM simulations, and the prediction of spreading Ti-6Al-4V powder on 79um substrate achieved at least 96% accuracy.

Zhang et al. (2017) proposed an ANN to interpolate the highly nonlinear relationships between spreader parameters (i.e., rotation speed and translation speed) and desired surface roughness and porosity of LB-PBF Ti-6Al-4V powder layers. The training data (35 samples) were also from the DEM simulation. A spreading process map was generated to determine spreader parameters to achieve the desired surface roughness with a prediction error of less than 3%, saving the total time for printing and reducing the build's cost.

ML in process—property relationship

LB-PBF process parameters significantly influence the product properties, such as density, tensile strength, yield strength, and fatigue performance, for reliable applications of LB-PBF. ML methods have been utilized as surrogate models to approximate the relationships between process parameters and product properties, as shown in Table 3.

The two major objectives of modeling process-property relationships include: (1) to discover the operating window for desired properties/performance; (2) to predict the final properties based on newly designed process parameters. There are three highlights for ML application in process-property relationship modeling:

(a) Interpretable ML and conventional ML are mainly used in modeling the process—property relationship compared with deep ML methods.
(b) Ensemble modeling with several conventional ML algorithms is a good practice to increase prediction accuracy.
(c) The same ML algorithm can be applied to predict different LB-PBF part properties in different models but with the same process parameters.

Process and performance optimization with LB-PBF part density

Modeling LB-PBF part density from process parameters is an early initiative in applying ML methods in LB-PBF studies. The early work mostly uses interpretable ML algorithms (such as linear regression) to explore the linear relationship between the process parameters and the density. For instance, Sun et al. (2013) applied a linear regression model to model the relationship between the density of LB-PBF Ti-6Al-4V specimens and four process parameters (i.e., laser energy density, hatch spacing, powder layer thickness, and scanning strategy). The specimens were built in sixteen different experiments (three specimens in each experiment) with varying process parameters designed by the Taguchi method. ANOVA was used to evaluate the significance of the impact of the four process parameters on the specimen density. The result showed that the powder layer thickness had the most significant impact on the density, while the hatch spacing was the least impactful. Their impact was modeled by a linear regression model to quantify the relationship and enable density prediction from these four process parameters with 8.1% relative error.

Aboulkhair et al. (2014) investigated the operating windows of parameters (scan speed, scan orientation, and hatch spacing) required to produce high-density parts from AlSi10Mg alloy using LB-PBF. The relative density of each of the built samples was determined by image processing of three cross-sectional optical micrographs, as in Fig. 9. These micrographs were used to quantify the evolution of pores with different hatch spacing, scan speed, and scan orientation. A compromise between the different parameters and scan strategies can produce parts, achieving a density of 99.8%.

Read et al. (2015) investigated the influence of process parameters of LB-PBF on the porosity development in the Al-Si10-Mg builds. 27 samples are printed under different parameter combinations (i.e., laser power, scan speed, hatch spacing, and island size) through a fractional factorial design. ANOVA was used to identify significant parameters and their interactions; then, second-order polynomial regression was fitted to describe the relationship between the process parameters and porosity with a high goodness of fit ($R^2 = 0.87$). It showed that either decreasing the laser power or increasing the scan speed could result in increased porosity.

Shah & Dey (2019) applied Taguchi design and ANOVA to investigate the effects of process parameters (laser power, scan speed, and hatch spacing) on density and ultimate tensile strength of LB-PBF AlSi10Mg components from 9 runs of experiments. The ANOVA results indicated that the hatch spacing had the most important effect on density. The Taguchi analysis found that laser power (followed by hatch spacing) was the most impactful on ultimate tensile strength. The best ultimate tensile strength and density were achieved with 1200 mm/s of scan speed, 0.15 mm of hatch spacing, and 330 W of laser power.

To achieve high-accuracy prediction, conventional ML methods, especially GP and ANNs, are adopted to model the relationship between density and process parameters. For instance, Tapia et al. (2016) proposed a GP-based predictive model for the learning and prediction of the density/porosity in LB-PBF 17–4 PH specimens from two process parameters: laser power and scanning speed. The model was trained by 42 specimens from a hypercube design and later improved by another 40 specimens to achieve prediction error < 20%. Furthermore, the case study results were instrumental in finding parameter combinations that result in high density in LB-PBF 17–4 PH specimens.

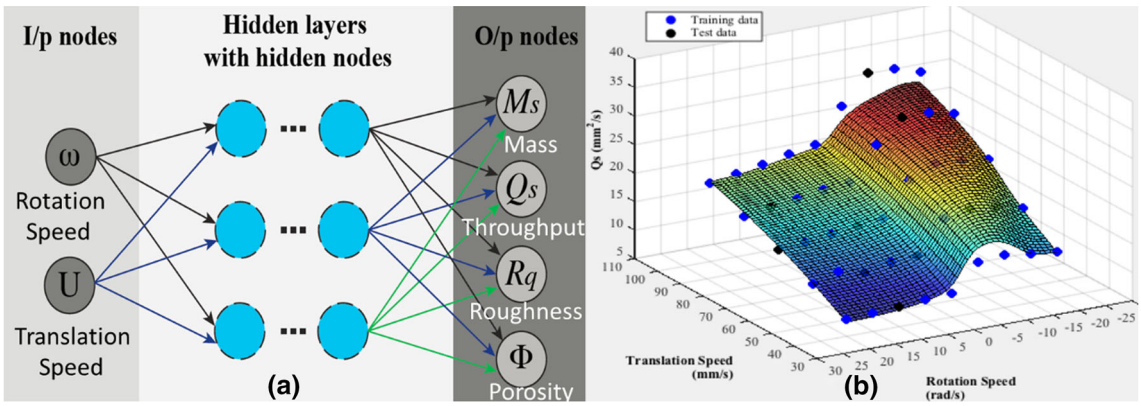

Fig. 8 **a** Schematic of an ANN for modeling the spread layer quality (such as spread throughput) for LB-PBF from process parameters of the spreader (such as spreader speeds); **b** regression surface of backpropagation ANN prediction for spread throughput of Ti-6Al-4V powder in LB-PBF (Desai & Higgs, 2019)

Table 3 ML applications to model and utilize process—property relationship in LB-PBF

Materials	Input	Output	Models	Categories	Data	References
Ti-6Al-4V	Laser energy density, hatch spacing, powder layer thickness, scanning strategy	Density	Linear regression	Interpretable ML	Experiment	Sun et al., (2013)
AlSi10Mg	Scan speed, scan orientation, hatch spacing	Density	Linear regression	Interpretable ML	Experiment	Aboulkhair et al., (2014)
AlSi10Mg	Laser power, scan speed, hatch spacing, island size	Density	Polynomial regression	Interpretable ML	Experiment	Read et al., (2015)
AlSi10Mg	Laser power, scan speed, hatch spacing	Density, ultimate tensile strength	Linear regression	Interpretable ML	Experiment	Shah & Dey, (2019)
17–4 PH	Laser power, scan speed	Density	GP	Conventional ML	Experiment	Tapia et al., (2016)
	Layer thickness, hatch spacing, laser power, scanning speed, environment temperature, interval time, scanning mode (SLS)	Density	ANN	Conventional ML	Experiment	Wang et al., (2009)
	Laser power, scan speed, scan spacing, layer thickness	Density	ANN	Conventional ML	Experiment	Shen et al., (2004)
Ti-6Al-4V	Laser power, scan speed, hatching distance, build orientation, building strategy, layer thickness	Density	Response surface methodology (RSM), ANN	Conventional ML	Experiment	Costa et al., (2022)
	Scanning speed, hatch spacing, laser pulse frequency	Density	Ensemble of regression, GP, SVM	Conventional ML	Experiment	Yang et al., (2018b)
316L SS	Laser power, scan speed, layer thickness	High cycle fatigue life	ANN	Conventional ML	Experiment	Zhang et al., (2019)
316L SS	Laser power, scan speed, layer thickness, hatch space	Fatigue life	ANN, random forest, SVM	Conventional ML	Simulation	Zhan & Li, (2021)
	Fatigue life from miniature specimens	Fatigue life	ANN	Conventional ML	Hybrid	Wan et al., (2019)
AlSi10Mg	Volumetric energy density, building orientation	Ultimate tensile strength, hardness, roughness	Optimal fuzzy regression	Conventional ML	Experiment	Ponticelli et al., (2020)

Table 3 (continued)

Materials	Input	Output	Models	Categories	Data	References
316L SS	Laser power, scan speed, hatch spacing, layer thickness	Density, hardness, surface roughness, ultimate tensile strength	Bayesian network	Conventional ML	Experiment	Hertlein et al., (2020)
AlSi10Mg	Hatch width, laser speed, laser power	Ultimate strength, yield strength, elongation	Diffusion maps	Conventional ML	Experiment	Marmarelis & Ghanem, (2020)
	Material composition, processing parameters (cooling rate, aging temperature, aging time)	Tensile yield strength, oxide precipitation, η precipitation strengthening, solid solution strengthening	Gaussian process	Conventional ML	Simulation	Yan et al., (2018)
Alloy 718	Build orientation, scan strategy, number of lasers, geometrical material descriptors	Porosity, creep rate	Ridge, LASSO, RF, Gradient boosted tree, SVR, DNN	Interpretable ML, Conventional ML, Deep ML	Experiment	Sanchez et al., (2021)
316L SS	Laser power, layer thickness, scanning speed	Powder utilization rate, energy consumption, tensile strength	Ensemble of GP, SVM, radial basis function (RBF)	Conventional ML	Experiment	Li et al., (2020)

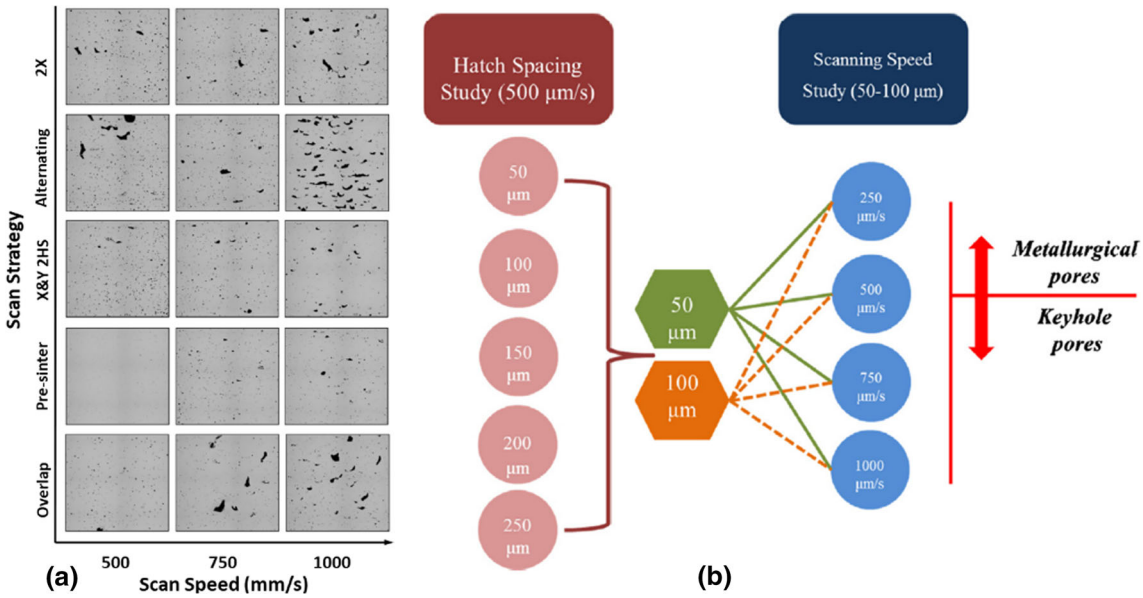

Fig. 9 **a** Porosity evolution in AlSi10Mg samples processed using different combinations of scan speeds and scan strategies; **b** hatch spacing, scan speed, and powder layer thickness are modeled linearly to predict the different pores in LB-PBF samples (Aboulkhair et al., 2014)

Wang et al. (2009) modeled the effects of process parameters on the density of the part prepared by selective laser sintering using an ANN. The ANN inputs were the process parameters, including layer thickness, hatch spacing, laser power, scanning speed, temperature of the working environment, interval time, and scanning mode. The prediction accuracy of ANN on part density was verified by the experimental data. Shen et al. (2004) also introduced an ANN approach for density prediction. Two-layer supervised neural networks were used, with the inputs to the neural network are LB-PBF process parameters such as laser power, scan speed, scan spacing, and layer thickness. The orthogonal experimental method was employed for collecting experimental training and test sets. Although the ANN model can analyze the relationship between the process parameters and the part density quantitatively, it was challenging to interpret the results. Costa et al. (2022) applied response surface methodology (RSM) and ANN to formulate two surrogate models to predict the density of Ti-6Al-4 V SLM manufactured parts from six process parameters (i.e., laser power, scan speed, hatching distance, build orientation, building strategy, layer thickness) and achieve 0.1 MAPE. They also used three nature-inspired optimization methods (i.e., self-adaptive harmony search, genetic algorithm, and particle swarm optimization) to optimize process parameters for high-density parts, which showed that the optimal ANN-based solutions took on smaller laser power values, higher hatching values and smaller scanning pattern angles than the RSM-based parameter configurations.

Furthermore, ensemble modeling is also used to increase the prediction accuracy in LB-PBF density. Yang et al. (2018b) aggregated three different ML algorithms (i.e., polynomial regression, kriging, and support vector machine) into a weighted composite in an ensemble model. They applied this ensemble model on an LB-PBF process to predict the relative density of parts from process parameters (scanning speed, hatch spacing, and laser pulse frequency). A total of 105 training data was generated from a fractional factorial design, and the prediction error was 5.47%, better than the individual algorithms in the ensemble.

LB-PBF part fatigue life prediction from process parameters with ML

The fatigue performance of LB-PBF parts is crucial in mission-critical and safety–critical applications. Since it is under the influence of numerous manufacturing parameters, conventional ML, especially ANNs, has been used as surrogate models to approximate the relationships between fatigue life and process parameters.

Zhang et al. (2019) predict the high cycle fatigue life of LB-PBF 316L stainless steel from process parameters (laser power, scan speed, and layer thickness) and post-processing treatments by using an ANN with fuzzy logic, as shown in Fig. 10a. The model was constructed from 18 experimental samples to map the complex nonlinear process-property relationship. Moreover, the authors also used the same ANN algorithm to develop a property-based model, as in Fig. 10b, with ultimate tensile strength and elongation to failure as input to predict the fatigue life. The two models performed well in fatigue life prediction with root mean square errors of less than 21%, as in Fig. 10c and d.

Zhan & Li (2021) predicted fatigue life of LB-PBF 316L stainless steel specimens from process parameters (including laser power, scan speed, hatch space, and powder layer thickness) with three ML models, namely, ANN, random forest (RF), and SVM. These ML models were trained by 70 simulations from the continuum damage mechanics technique and validated with experimental data from open publications. The results showed that fatigue life prediction with the SVM model could achieve ~ 15% relative error. To increase physics-based understanding and interpretability, parametric studies on fatigue life by changing each process parameter were implemented.

Moreover, Wan et al. (2019) proposed a potential roadmap to establish a data-driven evaluation platform for fatigue life prediction in metal additive manufacturing based on many miniature specimen-based experiment data, theoretical computations, and the 'big data' analysis with ML. They attempted to use ANNs to predict fatigue properties of a metal AM part from standard specimen tests and static mechanical properties of miniature specimens.

Process and performance optimization with multiple properties

Process and performance optimization can be achieved by modeling the relationships between process parameters and multiple properties of LB-PBF parts with the same ML algorithms. One advantage of ML surrogate models is their data-driven nature. They bypass the physics modeling, and instead project the input predictors (i.e., process parameters) to the output responses (i.e., properties) in a data-driven manner. As a convenient practice, multiple properties can be modeled simultaneously by the same ML algorithms from the same set of process parameters but with different model coefficients.

Interpretable ML models are widely used here. For instance, Ponticelli et al. (2020) Investigated the impacts on ultimate tensile strength, hardness, and roughness of LB-PBF AlSi10Mg specimens from process parameters (i.e., volumetric energy density and building orientation) by using optimal fuzzy regression. The fuzzy approach represented the optimal "imprecise" description of the relation between the parameters and the resulting quality. The model was trained by 30 specimens from a multi-level factorial design. The

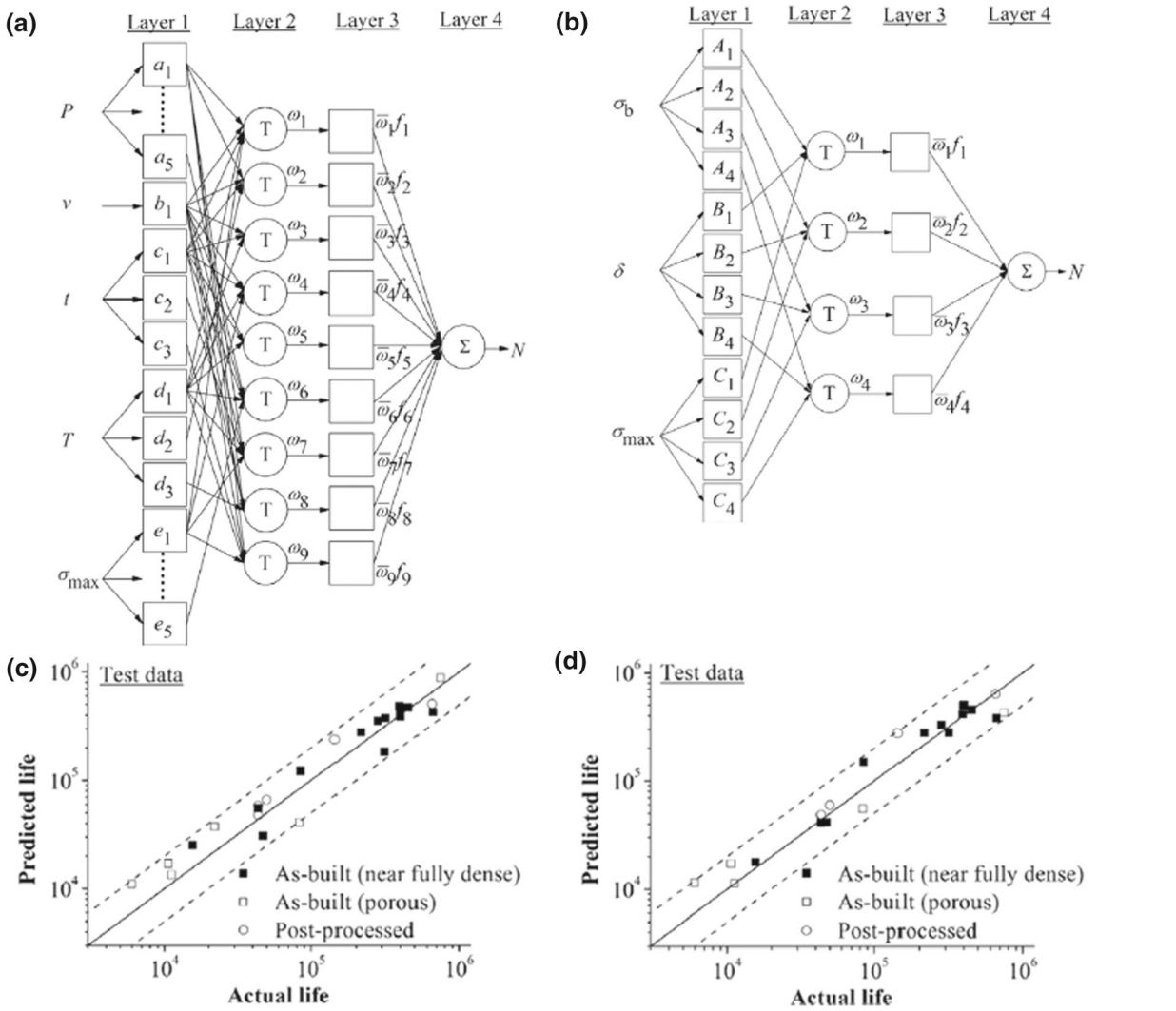

Fig. 10 Structure of the artificial neural network with fuzzy logic for **a** the "process-based" model and **b** the "property-based" model. Actual and predicted fatigue lives (load cycles) of the process-based model **c** and the property-based model (**d**). Dotted lines represent a factor of two on line (Zhang et al., 2019)

results were in close agreement with the experimental findings that volumetric energy density had a major influence only on the ultimate tensile strength, while interaction with the building orientation and the building orientation itself strongly affected the hardness and the roughness.

Hertlein et al. (2020) related four LB-PBF process parameters (laser power, scan speed, hatch spacing, and layer thickness) to five part quality characteristics (density, hardness, top layer surface roughness, ultimate tensile strength in the build direction and perpendicular to the build direction) of 316L stainless steel parts by using a Bayesian network, as shown in Fig. 11. This model was trained by 344 experimental data points mined from many publications. Based on the five quality characteristics, the predicted mean of hardness was within 0.41 standard deviation of the true value.

Conventional ML can model the complex process-property relationships with more flexibility than interpretable ML. For instance, Marmarelis & Ghanem (2020) inferred the dependence between LB-PBF process parameters (hatch width, laser speed, and power) and part properties (ultimate strength, yield strength, and elongation) of LB-PBF AlSi10Mg specimens by a novel adaptation of diffusion maps on an approximated Riemannian manifold. This model solved the curse of dimensionality in the manifold, and was trained with a small number of specimens (51). It allowed cost-effective prediction and optimization for the LB-PBF part properties based on process parameters with 65–70% certainty. To improve the interpretability with the first principles, the authors identified an efficient frontier of the

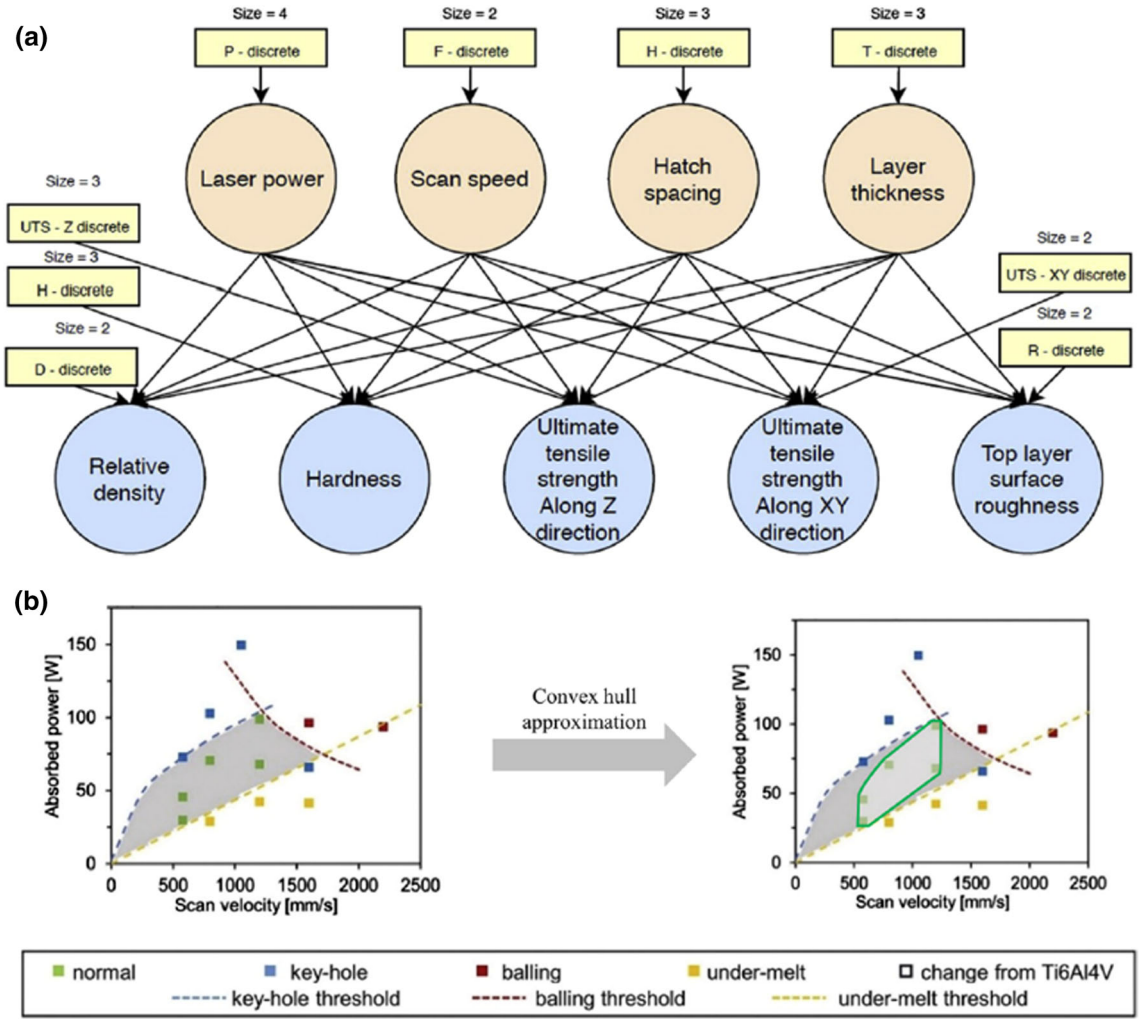

Fig. 11 **a** The final Bayesian network related four LB-PBF process parameters (laser power, scan speed, hatch spacing, and layer thickness) to five part quality characteristics (density, hardness, top layer surface roughness, ultimate tensile strength in the build direction and perpendicular to the build direction) of 316L stainless steel parts; **b** the feasible operating region of laser speed and power, shown in gray (Hertlein et al., 2020)

expectations of the three properties with respect to the process parameters.

By using GP, Yan et al. (2018) predicted mechanical properties (i.e., oxide precipitation, η precipitation strengthening, solid solution strengthening, and tensile yield strength) of LB-PBF specimens rapidly from material composition and processing parameters (cooling rate, aging temperature, aging time) of LB-PBF. Four GP-based models were developed from 200 simulated data points. They provided high-accuracy prediction (with errors ~ 0.23%) and dramatically reduced the prediction time from ~ 300 s (one physics-based mechanistic simulation) to a fraction of a second.

Sanchez et al. (2021) applied a variety of ML techniques (such as Ridge, LASSO, RF, Gradient boosted tree, SVR, DNN) to understand the effect of L-PBF process parameters on the creep rate of additively built nickel-based super alloy 718 and to predict the creep rate of the material from the process parameters and geometrical material descriptors extracted from optical microscope porosity images. The creep rate was accurately predicted with a percentage error of 1.40% in the best case, and the most important material descriptors were found to be part density, number of pores, build orientation and scan strategy.

Moreover, an ensemble model is used to increase the prediction accuracy for multiple LB-PBF part properties. For instance, Li et al. (2020) proposed an adaptive hybrid ensemble of three ML algorithms (kriging, radial basis function (RBF), and support vector regression (SVR)) to predict the powder utilization rate, the energy consumption, and the tensile strength of the as-built LB-PBF 316L stainless steel

specimens from the process parameters (i.e., laser power, layer thickness, scanning speed). The training data for these algorithms were 16 experiments from a Taguchi design, and the outputs from these three models on the LB-PBF responses were aggregated according to the local weights as the output of the proposed ensemble. The ensemble model improved the prediction accuracy of stand-alone algorithms by at least 20%.

ML in structure–property relationship

The structure–property relationship is also of great interest to understand the underlying physics of LB-PBF. ML surrogate models have been used to predict LB-PBF part properties, such as tensile strength, yield strength, with microstructure data, as in Table 4. Since the microstructure data (either captured by scanning electron microscopy (SEM), X-ray computed tomography (CT), or simulated) are two-dimensional or three-dimensional, there are two unique aspects for ML applications in structure–property relationship modeling:

(a) Data preprocessing and feature extraction by ML or by domain expertise are required before modeling. The interpretability of the ML surrogate model would depend on the extracted features.
(b) While images or 3-D structure data can be conveniently fed to deep ML algorithms, the interpretability of deep ML is challenging. In contrast, interpretable ML models with features designed from domain knowledge will be easy to interpret.

Kusano et al. (2020) predicted the tensile properties of heat-treated LB-PBF Ti-6Al-4V specimens from microstructures using multiple linear regression. A total of 48 specimens with 16 heat treatments were built, and their microstructures were captured by SEM (Scanning Electron Microscopy). The microstructural features were quantitatively extracted from the images by applying a random forest algorithm and image analysis techniques. They were then used in multiple linear regression analysis, together with defect-characterizing features from X-ray CT, to predict tensile properties. The results showed that the tensile property of LB-PBF Ti-6Al-4V alloy was strongly and intricately dependent on the microstructure (~ 0.82 correlation). However, since the microstructural features were extracted by random forest, it was difficult to further investigate how the microstructure affects the tensile properties.

Miyazaki et al. (Miyazaki et al., 2019) investigated the effects of heat treatments on mechanical properties (hardness) of LB-PBF Ti-6Al-4V samples from their microstructures. Nine different heat treatments were applied to LB-PBF Ti-6Al-4V samples, and the α particles in the microstructures were segmented by image processing and classified by random forest. It was found the distance between α particles gradually increased with heat treatment temperature, and the hardness tended to increase with the α particle width, area fraction, and nearest neighbor distances.

Herriott & Spear (2020) predicted yield strength of LB-PBF 316L stainless steel parts from a simulated microstructural dataset of ~ 7700 data points by applying ridge regression, gradient boosting, and convolutional neural network (CNN) based on VGGNet architecture. Morphological and crystallographic features were extracted from the simulated microstructural dataset as per-voxel or per-grain values. They served as the inputs for the ridge regression and gradient boosting models, while the CNN was trained with a 3D image of the microstructure (in Fig. 12). The computational efficiency for training the data-driven models was manageable (much less than the data simulation); for instance, (gradient boosting and ridge regression required ~ 3 min, CNN model required ~ 99 s per epoch). Once trained, each model predicted the yield strength in less than two seconds with high accuracy ($R^2 > 70\%$, RMSE ~ 20 MPa). Ridge regression was much more interpretable than gradient boosting and CNN.

Moreover, the manufacturability of an LB-PBF part can be assessed from its structure by using ML. For instance, Guo et al. (2020) proposed semi-supervised deep learning algorithms to assess the manufacturability of a metal cellular structure from its 3D CAD models. The proposed auto encoder-generative adversarial network (AE-GAN) classification model was built on deep convolutional GAN (DCGAN), and was trained by 50 randomly generated cellular structures in a semi-supervised setting with both labeled and unlabeled real structures. The proposed method can achieve ~ 80% accuracy in predicting the manufacturability of metal cellular structures. Mycroft et al. (2020) detailed a framework for predicting the printability of small-scale geometric features in AM by using machine learning (i.e., SVM, KNN, and random forest) to correlate 36 local geometry descriptors and printability.

Discussion and opportunities

With the rapid evolution of ML, growing deployment of LB-PBF, and exploding amount of sensor data, the integration of ML on LB-PBF as a tool for process and performance optimization has great traction in both academia and industry. This review has summarized different ML algorithms applied in LB-PBF to model the PSP relationships for process and performance optimization, as in Table 5. There are still opportunities for us to further promote applying ML to AM and fully unleash its potentials.

Table 4 ML applications to model and utilize structure—property relationship in LB-PBF

Materials	Input	Output	Models	Categories	Data	Refs
Ti-6Al-4V	Microstructure	Tensile strength	Multiple linear regression, random forest	Interpretable ML, Conventional ML	Experiment	Kusano et al., (2020)
Ti-6Al-4V	Microstructure	Hardness	Random forest	Conventional ML	Experiment	Miyazaki et al., (2019)
316L SS	Microstructure	Yield strength	Ridge regression, gradient boosting, CNN	Conventional ML, Deep ML	Simulation	Herriott & Spear, (2020)
	Cellular structure	Manufacturability	Generative adversarial network	Deep ML	Simulation	Guo et al., (2020)
Ti-6Al-4V	Geometry descriptors	Printability	Random forest, SVM, KNN	Conventional ML	Experiment	Mycroft et al., (2020)

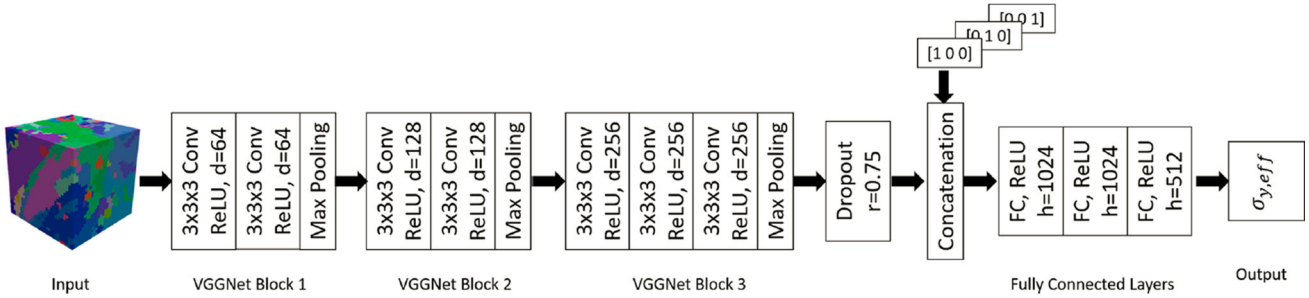

Fig. 12 Architecture of the 3D CNN based on VGGNet. It is trained with a 3D image of the microstructure to predict the yield strength of LB-PBF 316L stainless steel parts. The concatenation layer is optional and is only used when the load direction vector is included (Herriott & Spear, 2020)

Interpretability

To promote ML applications in LB-PBF, the interpretability of ML is strongly desired. Interpretability is a domain-specific notion. Not only can it help better understand model results, but also help to discover knowledge in LB-PBF.

From Table 5, it is noticed that conventional ML has been applied in process and performance optimization twice as much as interpretable ML and deep ML combined. Compared to interpretable ML models that can be interpreted conveniently to understand the process, conventional ML and deep ML constitute black-box models, having difficulties quantitatively interpreting the results. To explore the power of ML in discovering new knowledge and insights, interpretation with additional steps is needed for complex models from conventional ML and deep ML, such as model-agnostic methods, sensitivity analysis.

Currently, there are many research initiatives in increasing the interpretability of ML. For instance, DARPA launched its Explainable Artificial Intelligence (XAI) program in 2017 to develop new techniques capable of making intelligent systems explainable and delivering toolkits for defense or commercial applications (Gunning & Aha, 2019). NIST also initiates an Explainable AI workshop to discuss the principles of Explainable AI (Phillips et al., 2020). These initiatives indicate an irreversible trend to incorporate ML and AI into manufacturing and utilize these data-driven methods to explore the fundamental physics phenomena in manufacturing.

Standardization

Process and performance optimization in LB-PBF by ML is an interdisciplinary research area. To increase the effectiveness of ML applications in LB-PBF, deep integration and collaboration from various disciplines (such as materials science, mechanical engineering, ML) are needed. It requires both LB-PBF process expertise and strong ML knowledge to formulate a reasonable data-driven application with a suitable model due to the complexity of physics in LB-PBF.

However, current ML in LB-PBF is biased by the expertise of the practitioners, and is difficult to generate accurate and trustful integration. Some practitioners consider ML as off-the-shelf tools and miss the careful model tuning and hyperparameters selection; others lack adequate LB-PBF

Table 5 ML applications in LB-PBF. The most popular category is conventional ML, and the most used methods are GP and ANN in conventional ML and linear regression in interpretable ML

Categories	Methods	Parameter—Signatures	Process—Structure	Process—Property	Structure–Property	Total
Interpretable ML (**24**)	Linear regression	3	3	7	1	**14**
	Ridge regression	2		1	1	4
	Decision tree	2				2
	Bayesian network		1	1	2	4
Conventional ML (**59**)	Random forest	3	2	3	1	9
	Support vector machine	3	2	4	1	10
	Kernel regression	3		3	1	7
	Gaussian process	8	3	4		**15**
	Artificial neural network	1	6	6		**13**
	Gradient boost		1		1	2
	K-means clustering	1	2			3
Deep ML (**6**)	Autoencoder	1				1
	Convolutional neural network	1	1	1	1	4
	Generative adversarial network				1	1

The numbers in bold indicate the most popular ML methods in AM (i.e., GP, ANN and linear regression)

domain knowledge, and blindly apply ML without proper process interpretation and insights.

Therefore, standardization in ML applications in LB-PBF can facilitate practitioners to apply ML in their LB-PBF processes. Despite the differences in manufacturers, the same physics of LB-PBF could lead to potential standardization in sensing, data, feature extraction, simulation, model selection, and interpretation. Furthermore, one of the difficulties arising from ML algorithms involves tuning hyperparameters, developing standard parameters, or a standard method for tuning them (instead of the usual trial-and-error approach), which could lead to better ML models becoming industry standards. The standardization can help promote a systematic and reliable integration of ML in process and performance optimization in LB-PBF and advance the research within the community.

Collaborative platform

The limited amount of data for ML applications in LB-PBF hinders accurate results. Since ML is data-driven in nature, the reliability of its results is impacted by the quality and quantity of the data. However, due to the cost and time spent on each build and measurement, the available data for ML in LB-PBF in each study is not abundant. The simulated data is also often of high computation. Furthermore, using insufficient data to draw conclusions may lead to erroneous deductions. This is a particularly high risk when ML models are used by non-experts, unfamiliar with the pitfalls of issues such as over-fitting or failing to do cross-validation.

To fully exert the power of ML in LB-PBF applications, a collaborative platform for data sharing is desired. From the literature review, it is noticed that several research targets the same areas (e.g., melt pool geometry modeling from process parameters). If the experiment data from each study can be shared on a collaborative platform with necessary process settings in a standardized format, not only the practitioners

from both academia and industry can benefit from them for new applications, but also the researchers have sufficient data to verify their studies and carry out new research (Liu et al., 2021). Currently, NIST has built the Additive Manufacturing Materials Database (AMMD) from their experiments. Encouraging researchers to upload their experimental data in a standard format should be an efficient way to achieve the scale effect in the future.

Conclusions

The studies of machine learning (ML) for process and performance optimization in laser beam powder bed fusion (LB-PBF) in the recent decade are reviewed in this paper. These studies aimed to optimize process parameters and product properties/performance by leveraging and utilizing the process-structure–property relationships, modeled or approximated by a variety of ML algorithms or their ensemble. To facilitate a better understanding of the ML applications in LB-PBF, we proposed a new way to categorize the ML algorithms, i.e., interpretable ML, conventional ML, and deep ML on the interpretability and accuracy. For instance, interpretable ML is linear or rule-based, and is beneficial to learn or understand the physics in LB-PBF, while deep ML can model nonlinear relationships with high accuracy but low interpretability. This way is particularly useful for practitioners to select the ML algorithms according to their needs.

During the review, we carefully examined the three categories of ML in LB-PBF in their applications of modeling or approximating the relationships between process parameters and process signatures, between process and structure, between process and properties/performance, between structure and properties/performance. The review can serve as a comprehensive reference for the readers to know what the current ML applications are in the areas they want to investigate. The data used in the applications (from the experiment, simulation, or both) and feature extraction (manually or automatically) were also reviewed.

ML has become a useful tool to understand the LB-PBF process and predict product properties with different measurement data and simulations. In the future, enhancing the interpretability of ML, standardizing a systemic procedure for ML, and developing a collaborative platform to share data and findings will be critical to promote the integration of ML in LB-PBF applications on a large scale.

Funding This work was partially funded by the Federal Aviation Administration (FAA) under grant Nos. FAA-12-C-AM-AU-A2 & FAA-12-C-AM-AU-A3, and the National Science Foundation (NSF) under Grant No. NSF-CMMI-2134689.

References

"Additive Manufacturing Market by Technology" AMPOWER Report2020, Available: https://additive-manufacturing-report.com/additive-manufacturing-market/. Accessed Nov 2020.

"Broad Agency Announcement, Explainable Artificial Intelligence (XAI)," Defense Advanced Research Projects Agency, DARPA-BAA-16–53 (DARPA, 2016), 2016. https://www.darpa.mil/attachments/DARPA-BAA-16-53.pdf. Accessed Nov 2020.

Aboulkhair, N. T., Everitt, N. M., Ashcroft, I., & Tuck, C. (2014). Reducing porosity in AlSi10Mg parts processed by selective laser melting. *Additive Manufacturing, 1–4*, 77–86.

Adadi, A., & Berrada, M. (2018). Peeking inside the black-box: A survey on explainable artificial intelligence (XAI). *IEEE Access, 6*, 52138–52160.

Aoyagi, K., Wang, H., Sudo, H., & Chiba, A. (2019). Simple method to construct process maps for additive manufacturing using a support vector machine. *Additive Manufacturing, 27*, 353–362.

Bengio, Y., Courville, A., & Vincent, P. (2013). Representation learning: A review and new perspectives. *IEEE Transactions on Pattern Analysis and Machine Intelligence, 35*(8), 1798–1828.

Bishop, C. M. (2006). *Pattern recognition and machine learning*. Springer.

Breiman, L., Friedman, J., Stone, C. J., & Olshen, R. A. (1984). *Classification and regression trees*. CRC Press.

Cortes, C., & Vapnik, V. (1995). Support-vector networks. *Machine Learning, 20*(3), 273–297.

Costa, A., Buffa, G., Palmeri, D., Pollara, G., & Fratini, L. (2022). Hybrid prediction-optimization approaches for maximizing parts density in SLM of Ti6Al4V titanium alloy. *Journal of Intelligent Manufacturing*, *33*, 1967–1989. https://doi.org/10.1007/s10845-022-01938-9

Desai, P. S., & Higgs, C. F. (2019). Spreading process maps for powder-bed additive manufacturing derived from physics model-based machine learning. *Metals, 9*(11), 1176.

DeVor, R., Kapoor, S., Cao, J., & Ehmann, K. (2012). Transforming the landscape of manufacturing: distributed manufacturing based on desktop manufacturing (DM) 2. *Journal of manufacturing science and engineering, 134*(4), 041004.

Donegan, S. P., Schwalbach, E. J., & Groeber, M. A. (2020). Zoning additive manufacturing process histories using unsupervised machine learning. *Materials Characterization, 161*, 110123.

Drucker, H., Burges, C. J., Kaufman, L., Smola, A. J., & Vapnik, V. (1996). Support vector regression machines. *Advances in Neural Information Processing Systems, 9*, 155–161.

Everton, S. K., Hirsch, M., Stravroulakis, P., Leach, R. K., & Clare, A. T. (2016a). Review of in-situ process monitoring and in-situ metrology for metal additive manufacturing. *Materials Design, 95*, 431–445.

Everton, S. K., Hirsch, M., Stravroulakis, P., Leach, R. K., & Clare, A. T. (2016b). Review of in-situ process monitoring and in-situ metrology for metal additive manufacturing. *Materials & Design, 95*, 431–445.

Fatemi, A., et al. (2019). Fatigue behaviour of additive manufactured materials: An overview of some recent experimental studies on Ti-6Al-4V considering various processing and loading direction effects. *Fatigue & Fracture of Engineering Materials & Structures, 42*(5), 991–1009.

Ford, S., & Despeisse, M. (2016). Additive manufacturing and sustainability: An exploratory study of the advantages and challenges. *Journal of Cleaner Production, 137*, 1573–1587.

Freedman, D. A. (2009). *Statistical models: theory and practice*. Cambridge University Press.

Garg, A., Lam, J. S. L., & Savalani, M. M. (2015). A new computational intelligence approach in formulation of functional relationship of

open porosity of the additive manufacturing process. *The International Journal of Advanced Manufacturing Technology, 80*(1), 555–565.

Garland, A. P., White, B. C., Jared, B. H., Heiden, M., Donahue, E., & Boyce, B. L. (2020). Deep convolutional neural networks as a rapid screening tool for complex additively manufactured structures. *Additive Manufacturing, 35*, 101217.

Ghobadian, A., Talavera, I., Bhattacharya, A., Kumar, V., Garza-Reyes, J. A., & O'regan, N. (2020). Examining legitimatisation of additive manufacturing in the interplay between innovation, lean manufacturing and sustainability. *International Journal of Production Economics, 219*, 457–468.

Global Additive Manufacturing Market and Technology Forecast 2020-2028. Available: https://www.globenewswire.com/news-release/2020/09/15/2093525/0/en/Global-Additive-Manufacturing-Market-and-Technology-Forecast-2020-2028.html. Accessed Nov 2020.

Gockel, J., Sheridan, L., Koerper, B., & Whip, B. (2019). The influence of additive manufacturing processing parameters on surface roughness and fatigue life. *International Journal of Fatigue, 124*, 380–388.

Goh, G. D., Sing, L. S., & Yeong, Y. Y. (2021). A review on machine learning in 3D printing: Applications, potential, and challenges. *Artificial Intelligence Review, 54*(1), 63–94.

Goodfellow, I., Bengio, Y., & Courville, A. (2016). *Deep learning*. MIT press.

Gunning, D., & Aha, D. (2019). DARPA's explainable artificial intelligence (XAI) program. *AI Magazine, 40*(2), 44–58.

Guo, N., & Leu, M. C. (2013). Additive manufacturing: Technology, applications and research needs. *Frontiers of Mechanical Engineering, 8*(3), 215–243.

Guo, Y., Lu, W. F., & Fuh, J. Y. H. (2020). Semi-supervised deep learning based framework for assessing manufacturability of cellular structures in direct metal laser sintering process. *Journal of Intelligent Manufacturing, 32*(2), 347–359.

Herriott, C., & Spear, A. D. (2020). Predicting microstructure-dependent mechanical properties in additively manufactured metals with machine- and deep-learning methods. *Computational Materials Science, 175*, 109599.

Hertlein, N., Deshpande, S., Venugopal, V., Kumar, M., & Anand, S. (2020). Prediction of selective laser melting part quality using hybrid Bayesian network. *Additive Manufacturing, 32*, 101089.

Ho, T. K., (1995) "Random decision forests," In: *Proceedings of 3rd international conference on document analysis and recognition*, 1: 278–282: IEEE.

Hong, R., et al. (2020). Artificial neural network-based geometry compensation to improve the printing accuracy of selective laser melting fabricated sub-millimetre overhang trusses. *Additive Manufacturing, 37*, 101594.

Jordan, M. I. (2019). "Artificial intelligence—the revolution hasn't happened yet." *Harvard Data Science Review*, *1*(1). https://doi.org/10.1162/99608f92.f06c6e61

Kamath, C. (2016). Data mining and statistical inference in selective laser melting. *The International Journal of Advanced Manufacturing Technology, 86*(5), 1659–1677.

Kamath, C., & Fan, Y. J. (2018). Regression with small data sets: A case study using code surrogates in additive manufacturing. *Knowledge and Information Systems, 57*(2), 475–493.

Kappes, B., Moorthy, S., Drake, D., Geerlings, H., and Stebner, A., (2018) "Machine learning to optimize additive manufacturing parameters for laser powder bed fusion of Inconel 718." In: *Proceedings of the 9th International Symposium on Superalloy 718 & Derivatives: Energy, Aerospace, and Industrial Applications*, pp. 595–610: Springer.

King, W. E., et al. (2015). Laser powder bed fusion additive manufacturing of metals; physics, computational, and materials challenges. *Applied Physics Reviews, 2*(4), 041304.

Kusano, M., et al. (2020). Tensile properties prediction by multiple linear regression analysis for selective laser melted and post heat-treated Ti-6Al-4V with microstructural quantification. *Materials Science and Engineering: A, 787*, 139549.

Kwon, O., et al. (2020). A deep neural network for classification of melt-pool images in metal additive manufacturing. *Journal of Intelligent Manufacturing, 31*(2), 375–386.

Lee, J., Davari, H., Singh, J., & Pandhare, V. (2018). Industrial artificial intelligence for industry 4.0-based manufacturing systems. *Manufacturing Letters, 18*, 20–23.

Lee, S., Peng, J., Shin, D., & Choi, Y. S. (2019). Data analytics approach for melt-pool geometries in metal additive manufacturing. *Science and Technology of Advanced Materials, 20*(1), 972–978.

Le-Hong, T., Lin, P. C., Chen, J. -Z., Pham, T. D. Q., & Van Tran, X. (2021). Data-driven models for predictions of geometric characteristics of bead fabricated by selective laser melting. *Journal of Intelligent Manufacturing*. https://doi.org/10.1007/s10845-021-01845-5

Li, B., Hou, B., Yu, W., Lu, X., & Yang, C. (2017). Applications of artificial intelligence in intelligent manufacturing: A review. *Frontiers of Information Technology & Electronic Engineering, 18*(1), 86–96.

Li, J., Cao, L., Hu, J., Sheng, M., Zhou, Q., & Jin, P. (2020). A prediction approach of SLM based on the ensemble of metamodels considering material efficiency, energy consumption, and tensile strength. *Journal of Intelligent Manufacturing, 23*, 1–16.

Liu, J. (2017) "Heterogeneous sensor data based online quality assurance for advanced manufacturing using spatiotemporal modeling," Ph.D. Dissertation, Industrial and Systems Engineering, Virginia Polytechnic Institute and State University, Blacksburg, Virginia.

Liu, J., Liu, C., Bai, Y., Rao, P., Williams, C. B., & Kong, Z. (2019). Layer-wise spatial modeling of porosity in additive manufacturing. *IISE Transactions, 51*(2), 109–123.

Liu, S., Stebner, A. P., Kappes, B. B., & Zhang, X. (2021). Machine learning for knowledge transfer across multiple metals additive manufacturing printers. *Additive Manufacturing, 39*, 101877.

Markl, M., & Körner, C. (2016). Multiscale modeling of powder bed-based additive manufacturing. *Annual Review of Materials Research, 46*(1), 93–123.

Marmarelis, M. G., & Ghanem, R. G. (2020). Data-driven stochastic optimization on manifolds for additive manufacturing. *Computational Materials Science, 181*, 109750.

Masoomi, M., Pegues, J. W., Thompson, S. M., & Shamsaei, N. (2018). A numerical and experimental investigation of convective heat transfer during laser-powder bed fusion. *Additive Manufacturing, 22*, 729–745.

Meng, L., McWilliams, B., Jarosinski, W., Park, H.-Y., Jung, Y.-G., Lee, J., & Zhang, J. (2020). Machine learning in additive manufacturing: A review. *JOM Journal of the Minerals Metals and Materials Society, 72*(6), 2363–2377.

Meng, L., & Zhang, J. (2020). Process design of laser powder bed fusion of stainless steel using a Gaussian process-based machine learning model. *JOM Journal of the Minerals Metals and Materials Society, 72*(1), 420–428.

Miyazaki, S., Kusano, M., Bulgarevich, D. S., Kishimoto, S., Yumoto, A., & Watanabe, M. (2019). Image segmentation and analysis for microstructure and property evaluations on Ti–6Al–4V fabricated by selective laser melting. *Materials Transactions, 60*(4), 561–568.

Molaei, R., Fatemi, A., Sanaei, N., Pegues, J., Shamsaei, N., Shao, S., Li, P., Warner, D. H., & Phan, N. (2020). Fatigue of additive manufactured Ti-6Al-4V, Part II: The relationship between microstructure,

material cyclic properties, and component performance. *International Journal of Fatigue, 132*, 105363.
Molnar, C. (2020). *Interpretable machine learning : A guide for making black box models explainable* (2nd ed.). Independently Published.
Mondal, S., Gwynn, D., Ray, A., & Basak, A. (2020). Investigation of melt pool geometry control in additive manufacturing using hybrid modeling. *Metals, 10*(5), 683.
Mycroft, W., et al. (2020). A data-driven approach for predicting printability in metal additive manufacturing processes. *Journal of Intelligent Manufacturing, 31*(7), 1769–1781.
Olleak, A., & Xi, Z. (2020). Calibration and validation framework for selective laser melting process based on multi-fidelity models and limited experiment data. *Journal of Mechanical Design, 142*(8), 081701.
Park, H. S., Nguyen, D. S., Le-Hong, T., & Van Tran, X. (2022). Machine learning-based optimization of process parameters in selective laser melting for biomedical applications. *Journal of Intelligent Manufacturing, 33*(6), 1843–1858.
Paulson, N. H., Gould, B., Wolff, S. J., Stan, M., & Greco, A. C. (2020). Correlations between thermal history and keyhole porosity in laser powder bed fusion. *Additive Manufacturing, 34*, 101213.
Pegues, J. W., et al. (2020). Fatigue of additive manufactured Ti-6Al-4V, part I: The effects of powder feedstock, manufacturing, and post-process conditions on the resulting microstructure and defects. *International Journal of Fatigue, 132*, 105358.
Phillips, P. J., Hahn, C. A., Fontana, P. C., Broniatowski, D. A., & Przybocki, M. A. (2020). *Four principles of explainable artificial intelligence*. National Institute of Standards and Technology Interagency. https://tsapps.nist.gov/pub1555lication/get_pdf.cfm?pub_id=933399
Ponticelli, G. S., Giannini, O., Guarino, S., & Horn, M. (2020). An optimal fuzzy decision-making approach for laser powder bed fusion of AlSi10Mg alloy. *Journal of Manufacturing Processes, 58*, 712–723.
Popova, E., Rodgers, T. M., Gong, X., Cecen, A., Madison, J. D., & Kalidindi, S. R. (2017). Process-structure linkages using a data science approach: Application to simulated additive manufacturing data. *Integrating Materials and Manufacturing Innovation, 6*(1), 54–68.
Qi, X., Chen, G., Li, Y., Cheng, X., & Li, C. (2019). Applying neural-network-based machine learning to additive manufacturing: Current applications, challenges, and future perspectives. *Engineering, 5*(4), 721–729.
Rao, P. K., Liu, J., Roberson, and Kong, Z., (2015b) "Sensor-based online process fault detection in additive manufacturing." In: *International Manufacturing Science and Engineering Conference*, 56833, V002T04A010: American Society of Mechanical Engineers.
Rao, P. K., Liu, J. P., Roberson, D., Kong, Z. J., & Williams, C. (2015). Online real-time quality monitoring in additive manufacturing processes using heterogeneous sensors. *Journal of Manufacturing Science and Engineering, 137*(6), 061007.
Razvi, S. S., Feng, S., Narayanan, A., Lee, Y.-T. T., and Witherell, P., (2019) "A review of machine learning applications in additive manufacturing." In: *International Design Engineering Technical Conferences and Computers and Information in Engineering Conference*, 59179: V001T02A040: American Society of Mechanical Engineers.
Read, N., Wang, W., Essa, K., & Attallah, M. M. (2015). Selective laser melting of AlSi10Mg alloy: Process optimisation and mechanical properties development. *Materials & Design, 1980–2015*(65), 417–424.
"Recommendations for Strengthening American Leadership in Industries of the Future," The President's Council of Advisors on Science and Technology, 2000. https://science.osti.gov/-/media/_/pdf/about/pcast/202006/PCAST_June_2020_Report.pdf. Accessed Nov 2020.
Ren, Y., & Wang, Q. (2021). Gaussian-process based modeling and optimal control of melt-pool geometry in laser powder bed fusion. *Journal of Intelligent Manufacturing*. https://doi.org/10.1007/s10845-021-01781-4
RongJi, W., Xinhua, L., Qingding, W., & Lingling, W. (2009). Optimizing process parameters for selective laser sintering based on neural network and genetic algorithm. *The International Journal of Advanced Manufacturing Technology, 42*(11), 1035–1042.
Rudin, C. (2019). Stop explaining black box machine learning models for high stakes decisions and use interpretable models instead. *Nature Machine Intelligence, 1*(5), 206–215.
Russell, S., & Norvig, P. (2003). "*Artificial intelligence: A modern approach*" (2nd ed.). Prentice Hall.
Russell, R., Wells, D., Waller, J., Poorganji, B., Ott, E., Nakagawa, T., Sandoval, H., Shamsaei, N., & Seifi, M. (2019). *"Qualification and certification of metal additive manufactured hardware for aerospace applications." Additive manufacturing for the aerospace industry* (pp. 33–66). Elsevier.
Sadowski, M., Ladani, L., Brindley, W., & Romano, J. (2016). Optimizing quality of additively manufactured Inconel 718 using powder bed laser melting process. *Additive Manufacturing, 11*, 60–70.
Sames, W. J., List, F. A., Pannala, S., Dehoff, R. R., & Babu, S. S. (2016). The metallurgy and processing science of metal additive manufacturing. *International Materials Reviews, 61*(5), 315–360.
Sanchez, S., Rengasamy, D., Hyde, C. J., Figueredo, G. P., & Rothwell, B. (2021). Machine learning to determine the main factors affecting creep rates in laser powder bed fusion. *Journal of Intelligent Manufacturing, 32*(8), 2353–2373.
Scime, L., & Beuth, J. (2019). Melt pool geometry and morphology variability for the Inconel 718 alloy in a laser powder bed fusion additive manufacturing process. *Additive Manufacturing, 29*, 100830.
Shah, R. K., & Dey, P. P. (2019). Process parameter optimization of dmls process to produce AlSi10Mg components. *Journal of Physics: Conference Series, 1240*(1), 012011.
Shen, X., Yao J., Wang, Y., and Yang, J., (2004) "Density prediction of selective laser sintering parts based on artificial neural network." In: *International Symposium on Neural Networks (ISNN 2004)*: Springer, pp. 832–840
Shrestha, R., Shamsaei, N., Seifi, M., & Phan, N. (2019). An investigation into specimen property to part performance relationships for laser beam powder bed fusion additive manufacturing. *Additive Manufacturing, 29*, 100807.
Silbernagel, C., Aremu, A., & Ashcroft, I. (2019). Using machine learning to aid in the parameter optimisation process for metal-based additive manufacturing. *Rapid Prototyping Journal, 26*(4), 625–637.
Smith, J., et al. (2016). Linking process, structure, property, and performance for metal-based additive manufacturing: Computational approaches with experimental support. *Computational Mechanics, 57*(4), 583–610.
Snell, R., et al. (2020). Methods for rapid pore classification in metal additive manufacturing. *JOM Journal of the Minerals Metals and Materials Society, 72*(1), 101–109.
Soltani-Tehrani, A., Pegues, J., & Shamsaei, N. (2020). Fatigue behavior of additively manufactured 17–4 PH stainless steel: The effects of part location and powder re-use. *Additive Manufacturing, 36*, 101398.
Srinivasan, S., Swick, B., & Groeber, M. A. (2020). Laser powder bed fusion parameter selection via machine-learning-augmented process modeling. *JOM*, *72*, 4393–4403.
"Strategy for American Leadership in Advanced Manufacturing". (2018). The National Science & Technology Council. Available: https://trumpwhitehouse.archives.gov/wp-content/uploads/2018/

10/Advanced-Manufacturing-Strategic-Plan-2018.pdf. Accessed Nov 2020.

Sun, J., Yang, Y., & Wang, D. (2013). Parametric optimization of selective laser melting for forming Ti6Al4V samples by Taguchi method. *Optics & Laser Technology, 49*, 118–124.

Tapia, G., & Elwany, A. (2014). A review on process monitoring and control in metal-based additive manufacturing. *Journal of Manufacturing Science and Engineering*. https://doi.org/10.1115/1.4028540

Tapia, G., Elwany, A. H., & Sang, H. (2016). Prediction of porosity in metal-based additive manufacturing using spatial Gaussian process models. *Additive Manufacturing, 12*, 282–290.

Tapia, G., Khairallah, S., Matthews, M., King, W. E., & Elwany, A. (2018). Gaussian process-based surrogate modeling framework for process planning in laser powder-bed fusion additive manufacturing of 316L stainless steel. *The International Journal of Advanced Manufacturing Technology, 94*(9), 3591–3603.

Tegmark, M. (2017). *Life 3.0: Being human in the age of artificial intelligence* (1st ed.). Knopf Doubleday Publishing Group.

Tibshirani, R. (1996). Regression shrinkage and selection via the lasso. *Journal of the Royal Statistical Society: Series B (methodological), 58*(1), 267–288.

Vulimiri, P., To, A., Zhang, X., Brice, C., Kappes, B., & Stebner, A. (2020). Invited review: Machine learning for materials developments in metals additive manufacturing. *Additive Manufacturing, 36*, 101641.

Wan, H. Y., Chen, G. F., Li, C. P., Qi, X. B., & Zhang, G. P. (2019). Data-driven evaluation of fatigue performance of additive manufactured parts using miniature specimens. *Journal of Materials Science & Technology, 35*(6), 1137–1146.

Wang, C., Tan, X. P., Tor, S. B., & Lim, C. S. (2020). Machine learning in additive manufacturing: State-of-the-art and perspectives. *Additive Manufacturing, 36*, 101538.

Wang, R., Li, J., Wang, F., Li, X., & Wu, Q. (2009). ANN model for the prediction of density in selective laser sintering. *International Journal of Manufacturing Research, 4*(3), 362–373.

Yadollahi, A., & Shamsaei, N. (2017). Additive manufacturing of fatigue resistant materials: Challenges and opportunities. *International Journal of Fatigue, 98*, 14–31.

Yadollahi, A., Shamsaei, N., Thompson, S. M., Elwany, A., & Bian, L. (2017). Effects of building orientation and heat treatment on fatigue behavior of selective laser melted 17–4 PH stainless steel. *International Journal of Fatigue, 94*, 218–235.

Yan, F., Chan, Y., Saboo, A., Shah, J., Olson, G. B., & Chen, W. (2018). Data-driven prediction of mechanical properties in support of rapid certification of additively manufactured alloys. *Computer Modeling in Engineering & Sciences, 117*(3), 343–366.

Yang, Z., Eddy, D., Krishnamurty, S., Grosse, I., and Lu, Y., (2018b) "A Super-Metamodeling Framework to Optimize System Predictability." In: *International Design Engineering Technical Conferences and Computers and Information in Engineering Conference*, 51722, V01AT02A009: American Society of Mechanical Engineers.

Yang, H. J., Hwang, P. J., & Lee, S. H. (2002). A study on shrinkage compensation of the SLS process by using the Taguchi method. *International Journal of Machine Tools and Manufacture, 42*(11), 1203–1212.

Yang, Z., Eddy, D., Krishnamurty, S., Grosse, I., Denno, P., Witherell, PW., Lopez, F., (2018a). Dynamic metamodeling for predictive analytics in advanced manufacturing. *Smart and Sustainable Manufacturing Systems, 2*(1), 18–39.

Zhan, Z., & Li, H. (2021). Machine learning based fatigue life prediction with effects of additive manufacturing process parameters for printed SS 316L. *International Journal of Fatigue, 142*, 105941.

Zhang, C., & Ma, Y. (2012). *Ensemble machine learning: methods and applications*. Springer.

Zhang, W., Mehta, A., Desai, P. S., and Higgs, C., (2017) "Machine learning enabled powder spreading process map for metal additive manufacturing (AM)." In: *Int. Solid Free Form Fabr. Symp. Austin, TX*, pp. 1235–1249.

Zhang, M., et al. (2019). High cycle fatigue life prediction of laser additive manufactured stainless steel: A machine learning approach. *International Journal of Fatigue, 128*, 105194.